REPORT DOCUMENTATION PAGE

Form Approved OMB NO. 0704-0188

The public reporting burden for this collection of information is estimated to average 1 hour per response, including the time for reviewing instructions, searching existing data sources, gathering and maintaining the data needed, and completing and reviewing the collection of information. Send comments regarding this burden estimate or any other aspect of this collection of information, including suggesstions for reducing this burden, to Washington Headquarters Services, Directorate for Information Operations and Reports, 1215 Jefferson Davis Highway, Suite 1204, Arlington VA, 22202-4302. Respondents should be aware that notwithstanding any other provision of law, no person shall be subject to any oenalty for failing to comply with a collection of information if it does not display a currently valid OMB control number.
PLEASE DO NOT RETURN YOUR FORM TO THE ABOVE ADDRESS.

1. REPORT DATE (DD-MM-YYYY)	2. REPORT TYPE	3. DATES COVERED (From - To)
31-03-2013	Final Report	1-Apr-2012 - 31-Dec-2012

4. TITLE AND SUBTITLE
Earth-abundant materials as photosensitizers in the molecular assemblies for
solar energy conversion

5a. CONTRACT NUMBER
W911NF-12-1-0116

5b. GRANT NUMBER

5c. PROGRAM ELEMENT NUMBER
611102

6. AUTHORS
Elena Jakubikova

5d. PROJECT NUMBER

5e. TASK NUMBER

5f. WORK UNIT NUMBER

7. PERFORMING ORGANIZATION NAMES AND ADDRESSES
North Carolina State University
Research Administration
2701 Sullivan Drive, Suite 240
Raleigh, NC 27695 -7514

8. PERFORMING ORGANIZATION REPORT NUMBER

9. SPONSORING/MONITORING AGENCY NAME(S) AND ADDRESS(ES)
U.S. Army Research Office
P.O. Box 12211
Research Triangle Park, NC 27709-2211

10. SPONSOR/MONITOR'S ACRONYM(S)
ARO

11. SPONSOR/MONITOR'S REPORT NUMBER(S)
59842-CH-II.3

12. DISTRIBUTION AVAILIBILITY STATEMENT
Approved for Public Release; Distribution Unlimited

13. SUPPLEMENTARY NOTES
The views, opinions and/or findings contained in this report are those of the author(s) and should not contrued as an official Department of the Army position, policy or decision, unless so designated by other documentation.

14. ABSTRACT
We investigate the applicability of the B3LYP functional to the ground state determination of first row transition metal complexes, focusing mainly on Fe(II)-polypyridine complexes with ligands of varying ligand field strength. We find that the error in the energy differences between the low-spin (singlet) and high-spin (quintet) states is systematic for structurally related complexes that undergo similar distortion in the metal-ligand coordination environment between the high-spin and low-spin states. This systematic behavior can be exploited and the ground

15. SUBJECT TERMS
iron(II) polypyridines, photosensitizers, band-selective sensitization, density functional theory, spin-crossover, B3LYP

16. SECURITY CLASSIFICATION OF:			17. LIMITATION OF ABSTRACT	15. NUMBER OF PAGES	19a. NAME OF RESPONSIBLE PERSON
a. REPORT	b. ABSTRACT	c. THIS PAGE			Elena Jakubikova
UU	UU	UU	UU		19b. TELEPHONE NUMBER 919-515-1808

Report Title

Earth-abundant materials as photosensitizers in the molecular assemblies for solar energy conversion

ABSTRACT

We investigate the applicability of the B3LYP functional to the ground state determination of first row transition metal complexes, focusing mainly on Fe(II)-polypyridine complexes with ligands of varying ligand field strength. We find that the error in the energy differences between the low-spin (singlet) and high-spin (quintet) states is systematic for structurally related complexes that undergo similar distortion in the metal-ligand coordination environment between the high-spin and low-spin states. This systematic behavior can be exploited and the ground state of an arbitrary Fe(II) complex can be determined by comparing the calculated energy differences between the singlet and quintet electronic states of a complex to the energy differences of structurally related complexes with a known, experimentally-determined ground state. Furthermore, we apply DFT and TD-DFT to study ground and excited state properties of Fe(II)-polypyridine sensitizers. Quantum dynamics simulations are further used to investigate the interfacial electron transfer (IET) between the excited Fe(II) dyes and titanium dioxide nanoparticle. All three complexes investigated display band-selective sensitization, whose origin is attributed to the poor alignment of the lowest energy excited states with the conduction band of the titanium dioxide semiconductor.

Enter List of papers submitted or published that acknowledge ARO support from the start of the project to the date of this printing. List the papers, including journal references, in the following categories:

(a) Papers published in peer-reviewed journals (N/A for none)

Received		Paper
02/28/2013	1.00	Elena Jakubikova, David N. Bowman. Low-Spin versus High-Spin Ground State in Pseudo-Octahedral Iron Complexes, Inorganic Chemistry, (06 2012): 6011. doi: 10.1021/ic202344w
TOTAL:		**1**

Number of Papers published in peer-reviewed journals:

(b) Papers published in non-peer-reviewed journals (N/A for none)

Received		Paper
TOTAL:		

Number of Papers published in non peer-reviewed journals:

(c) Presentations

1. E. Jakubikova, ”Toward computational design of iron-based chromophores for photovoltaics,” Electron Donor-Acceptor Interactions GRC, August 5-10, 2012 (oral).
2. E. Jakubikova, "Earth-abundant solar cells: Can iron complexes serve as photosensitizers in DSSCs?" The Southeastern Regional Meeting of the American Chemical Society in Raleigh, November 14-17, 2012 (oral).
3. D. N. Bowman, L. J. Barnes, T. Tsuchiya, E. Jakubikova, "Toward computational design of iron-based chromophores for photovoltaics," 21st Conference on Current Trends in Computational Chemistry in Jackson, MS, November 9-10, 2012 (poster).
4. D. N. Bowman, R. C. Rocha, E. Jakubikova, "Reproducing solvatochromic behavior in cyano-containing chromophores: Explicit solvent vs. implicit model," The Southeastern Regional Meeting of the American Chemical Society in Raleigh, November 14-17, 2012 (poster).
5. D. N. Bowman, R. C. Rocha, E. Jakubikova, "Reproducing solvatochromic behavior in cyano-containing chromophores: Explicit solvent vs. implicit model," North Carolina ACS local section meeting, November 14, 2012 (poster).
6. L. J. Barnes, D. N. Bowman, E. Jakubikova, "A computational study of electronic excitations in Fe(II)-polypyridines in the visible light region," North Carolina State University 21st Annual Undergraduate Research Symposium (Raleigh, NC), April 10, 2012 (poster).
7. L. J. Barnes, D. N. Bowman, T. Tsuchiya, E. Jakubikova, "Hydroxamate Linker Results in Fastest Interfacial Electron Transfer Rates in Fe(bpy)2(CN)2 - Sensitized Solar Cell," 11th Annual Summer Undergraduate Research Symposium, North Carolina State University, August 1, 2012 (poster).
8. L. J. Barnes, D. N. Bowman, T. Tsuchiya, E. Jakubikova, "Hydroxamate Linker Results in Fastest Interfacial Electron Transfer Rates in Fe(bpy)2(CN)2 - Sensitized Solar Cell," The Southeastern Regional Meeting of the American Chemical Society in Raleigh, November 14-17, 2012 (poster).

Number of Presentations: 8.00

Non Peer-Reviewed Conference Proceeding publications (other than abstracts):

Received	Paper

TOTAL:

Number of Non Peer-Reviewed Conference Proceeding publications (other than abstracts):

Peer-Reviewed Conference Proceeding publications (other than abstracts):

Received	Paper

TOTAL:

Number of Peer-Reviewed Conference Proceeding publications (other than abstracts):

(d) Manuscripts

Received	Paper	
03/29/2013	2.00	Elena Jakubikova, David N. Bowman, Takashi Tsuchiya, James H. Blew. Elucidating band-selective sensitization in iron(II) polypyridine-TiO2 assemblies, Inorganic Chemistry (03 2013)

TOTAL: **1**

Number of Manuscripts:

Books

Received	Paper	

TOTAL:

Patents Submitted

Patents Awarded

Awards

Graduate Students

NAME	PERCENT_SUPPORTED	Discipline
Sriparna Mukherjee	1.00	
FTE Equivalent:	**1.00**	
Total Number:	**1**	

Names of Post Doctorates

NAME	PERCENT_SUPPORTED
Takashi Tsuchiya	0.30
FTE Equivalent:	**0.30**
Total Number:	**1**

Names of Faculty Supported

NAME	PERCENT_SUPPORTED	National Academy Member
Elena Jakubikova	0.10	
FTE Equivalent:	**0.10**	
Total Number:	**1**	

Names of Under Graduate students supported

NAME	PERCENT_SUPPORTED	Discipline
Lyndsay Barnes	0.20	Chemical Engineering
FTE Equivalent:	**0.20**	
Total Number:	**1**	

Student Metrics

This section only applies to graduating undergraduates supported by this agreement in this reporting period

The number of undergraduates funded by this agreement who graduated during this period:	0.00
The number of undergraduates funded by this agreement who graduated during this period with a degree in science, mathematics, engineering, or technology fields:	0.00
The number of undergraduates funded by your agreement who graduated during this period and will continue to pursue a graduate or Ph.D. degree in science, mathematics, engineering, or technology fields:	0.00
Number of graduating undergraduates who achieved a 3.5 GPA to 4.0 (4.0 max scale):	0.00
Number of graduating undergraduates funded by a DoD funded Center of Excellence grant for Education, Research and Engineering:	0.00
The number of undergraduates funded by your agreement who graduated during this period and intend to work for the Department of Defense	0.00
The number of undergraduates funded by your agreement who graduated during this period and will receive scholarships or fellowships for further studies in science, mathematics, engineering or technology fields:	0.00

Names of Personnel receiving masters degrees

NAME
Total Number:

Names of personnel receiving PHDs

NAME
Total Number:

Names of other research staff

NAME	PERCENT_SUPPORTED
FTE Equivalent:	
Total Number:	

Sub Contractors (DD882)

Inventions (DD882)

Scientific Progress

see attachment

Technology Transfer

Proposal Title: Earth-abundant materials as photosensitizers in the molecular assemblies for solar energy conversion

Report Period Begin Date: 04/01/2012
Report Period End Date: 12/31/2012

1. Foreword

The Sun is an abundant source of energy capable of meeting all our energy needs if properly harvested. However, efficient capture, storage and transport of energy from sunlight still remain a challenge. One of the ways to utilize solar energy is conversion of sunlight to electricity via dye-sensitized solar cells (DSSCs) or to chemical fuels via photocatalytic synthetic cells. These systems are often designed around a single photoactive molecule (a chromophore) or a molecular array anchored to a semiconductor. The conversion of sunlight to electricity occurs via absorption of light by the chromophore, followed by the interfacial electron transfer (IET) between the chromophore and semiconductor. The most successful class of chromophores used in the molecular assemblies for solar energy conversion is based on Ru(II)-polypyridine compounds.[1] Unfortunately, ruthenium is a rare and expensive metal, which is one of the limiting factors to its wide application in the DSSCs or in photocatalytic assemblies.

Several first row transition metal complexes have been investigated as potential photosensitizers, among them iron and copper coordination compounds.[2-4] Our studies focus on Fe(II) polypyridine complexes due to their close relationship with the very successful Ru(II)-polypyridines. Additionally, Fe(II) coordination compounds have been studied in their role as photosensitizers experimentally by several research groups,[3-8] which provide us with a starting point and a set of benchmarks for our theoretical calculations.

In this report, we describe the results of our efforts to: (1) ***Evaluate DFT*** as a tool for calculations of Fe(II) complexes and show that it is an adequate tool to study their ground and excited state properties. (2) ***Obtain a better understanding of the previous experimental findings*** on Fe(II) complexes investigated as photosensitizers and published in the literature.[3-8] Our results provide an explanation for the band-selective electron injection phenomena in Fe(II)-polypyridine-TiO_2 nanoparticle assemblies and provide a pathway toward the design of more efficient Fe(II)-based chromophores.

2. Table of Contents

1. Foreward…… 1
2. Table of Contents……..... 2
3. List of Appendices, Illustrations, and Tables…… 3
4. Statement of the problem studied……... 5
5. Summary of the most important results…… 6
6. Conclusion…….. 13
7. Bibliography……... 15
8. Tables……..20
9. Figure Captions…….. 23
10. Figures…… 24

3. List of Appendices, Illustrations, and Tables

Table 1. Experimental and calculated spin multiplicity of pseudo-octahedral first row transition metal complexes investigated in this work. * denotes thermal spin crossover complexes.

Table 2. Table of average change in metal – ligand bond lengths ΔR(metal-ligand) in Ångstroms for low spin to high spin transition versus slope of the scan over the exact exchange for various pseudo-octahedral complexes. * $[Os(bpy)_3]^{2+}$ quintet changes electronic states over the exact exchange admixture investigated.

Table 3. Table of metal ligand bond lengths for the complexes investigated, coordination site labeling corresponds with Figure 6.

Figure 1. Fe(II) complexes investigated in this work.

Figure 2. Heteropyridine ligands considered in this study.

Figure 3. Dependence of the energy difference, $\Delta E_{HS/LS} = E_{high-spin} - E_{low-spin}$ (kcal/mol), on the exact exchange admixture (c_1) in the B3LYP functional for iron pseudo-octahedral complexes with various ligands: $[Fe(CN)_6]^{4-}$ (1), $[Fe(bpy)_2(CN)_2]^0$ (2), $[Fe(bpy)_3]^{2+}$ (3), $[Fe(NH_3)_6]^{3+}$ (4), $[FeCl_6]^{3-}$ (5). $\Delta E_{HS/LS} > 0$ corresponds to the low-spin ground state (singlet or doublet), $\Delta E_{HS/LS} < 0$ corresponds to the high-spin ground state (quintet or sextet).

Figure 4. Plot of average change in metal to ligand bond lengths in transition from low-spin to high-spin states versus slope of the scan over exact exchange for data shown in Table 2 along with a plot of the linear regression, R^2=0.93.

Figure 5. Dependence of the energy difference, $\Delta E_{HS/LS} = E_{high-spin} - E_{low-spin}$ $\Delta E_{HS/LS} = E_{high-spin} - E_{low-spin}$ (kcal/mol), on the exact exchange admixture (c_1) in the B3LYP functional for several pseudo-octahedral iron(II)-polypyridine complexes: $[Fe(bpy)_2(CN)_2]^0$ (**1**), $[Fe(bpy)_3]^{2+}$ (**2**), $[Fe(tren(py)_3)]^{2+}$ (**3**), $[Fe(bpy)_2(NCS)_2]^0$ (**4**), $[Fe(tren(6\text{-}Me\text{-}py)_3)]^{2+}$ (**5**), and $[Fe(bpy)_2Cl_2]^0$ (**6**). $\Delta E_{HS/LS} > 0$ $\Delta E_{HS/LS} > 0$ corresponds to the singlet ground state, $\Delta E_{HS/LS} < 0$ $\Delta E_{HS/LS} < 0$ corresponds to the quintet ground state. A linear regression is plotted for each complex based on the constant slope formula $\Delta E_{HS/LS} = I - 140.2c_1$.

Figure 6. Optimized structures of dyes **1**, **2**, and **3** with each coordination site labeled (L1-L6).

Figure 7. Simulated absorption spectra for (from top to bottom) dyes **1, 2**, and **3** with Lorentzian broadening of HWMH = 0.12 eV with important excitations ($f_{osc} > 0.01$) in the visible region labeled, calculated with B3LYP TD-DFT in PCM (acetonitrile).

Figure 8. Relevant particle states for the major excitations ($f_{osc} > 0.01$) from the calculated spectra shown in Figure 7. Kohn-Sham orbitals are classified by the absorption band (columns) and by similarity in nodal structure (rows).

Figure 9. Optimized structures of anatase (101) with pyridine-4-carboxylic acid binding via a monodentate (a) and bidentate (b) binding mode, and hydrogen cyanide (c).

Figure 10. Final slab models of dye-nanoparticle assemblies consisting of $[Fe(bpy\text{-}dca)_2(CN)_2]$ attached to anatase (101) via a monodentate carboxylic acid binding mode in the following nonequivalent orientations: bpy parallel (left) and bpy perpendicular (right).

Figure 11. Structure of **1**-TiO_2 assembly employing CN^- as the anchoring group.

Figure 12. Density of states for **1**-TiO_2 anatase (101) slab model (left) and enlarged conduction band (right) show the following: total density of states (blue line), projected density of states on the dye (black line), and the energy levels of the dye in vacuum using extended Hückel (black level set lines). Gaussian line-shape (HWHM = 0.05 eV) used for convolution.

Figure 13. Discrete energy levels of the dyes (left) in vacuum, using extended Hückel level of theory, showing the evolution of the similar molecular orbitals, going from the smallest to the largest dye. The DOS/pDOS for the $[Fe(bpy\text{-}dca)_2(CN)_2]/TiO_2$ nanoparticle system is shown for reference (right).

Figure 14. Characteristic interfacial electron transfer times for relevant particle states of $[Fe(bpy)(CN)_4]^{2-}$ attached to anatase (101) slab in both the "bpy parallel" and "bpy perpendicular" orientations via monodentate cyanide anchoring groups with varying nitrogen titanium distances (2.33, 2.22, and 2.12 Å), determined by either exponential or biexponential fitting.

Figure 15. Characteristic interfacial electron transfer times for relevant particle states of $[Fe(bpy\text{-}dca)(CN)_4]^{2-}$ attached to anatase (101) slab by monodentate carboxylic acid, bidentate carboxylic acid, and cyanide anchoring groups (in both the "bpy parallel" and "bpy perpendicular" orientations), determined by either exponential or biexponential fitting.

Figure 16. Characteristic interfacial electron transfer times for relevant particle states of $[Fe(bpy\text{-}dca)_2(CN)_2]$ attached to anatase (101) slab by monodentate carboxylic acid (in both the "bpy parallel" and "bpy perpendicular" orientations), bidentate carboxylic acid (in both the "bpy parallel" and "bpy perpendicular" orientations), and cyanide anchoring groups, determined by either exponential or biexponential fitting.

4. Statement of the Problem Studied

Iron pseudo-octahedral complexes have been long considered ideal building blocks for molecular electronic switches, data storage materials, or display devices.[9] Iron, as a first row transition metal, provides a weak ligand field in a pseudo-octahedral environment, which leads to the presence of two energetically close electronic states, ^{1}A and ^{5}T. Depending on the character of ligands coordinated to the central iron metal, the complexes can display either a low-spin (^{1}A), or a high-spin (^{5}T) ground state. The presence of a low-lying excited state of a different spin than the ground state is also responsible for the spin crossover phenomenon in these compounds, in which the complex changes its spin state under the application of an external perturbation such as a change in temperature, pressure, or exposure to electromagnetic radiation.[10]

Fe(II)-polypyridine complexes have also been investigated as **potential photosensitizers in dye-sensitized solar cells** due to their structural resemblance to the Ru(II)-polypyridine dyes and the low cost and low toxicity of iron.[11-16] The ability of Fe(II) polypyridines to serve as photosensitizers in DSSCs was first demonstrated by Ferrere and Gregg, although their efficiency is much lower than that of their Ru analogs.[13] While they initially absorb visible light into similar metal-to-ligand charge-transfer (MLCT) states as Ru(II)-polypyridines, the photoactive MLCT states undergo intersystem crossing (ISC) into the low-lying high-spin metal-centered states on sub-picosecond time scale.[16] Therefore, the interfacial electron transfer (IET) between the excited dye and semiconductor occurs only from the initially populated "hot" MLCT states. Since the lifetime of the MLCT manifold of these systems is approximately 100 fs,[16-18] the IET must occur with a characteristic time of approximately 100 fs or less in order to be competitive with the ultrafast ISC events.

The work of Ferrere and Gregg also established the band-selective behavior of the IET between the short-lived excited MLCT states of $Fe(bpy\text{-}dca)_2(CN)_2$ (bpy-dca = 2,2'-bipyridine-4,4'-dicarboxylic acid) and TiO_2 semiconductor.[13] Ferrere et al. observed that upon the initial excitation with visible light, the IET is more efficient (10-11%) from the higher energy MLCT band and much less efficient (2%), from the lower energy MLCT transitions.

Computational studies of Fe(II)-complexes aiming to either obtain a deeper understanding of their electronic structure or to suggest new compounds with desirable properties face a number of challenges. One of these challenges is the correct determination of the ground state, which is non trivial.[19-20] There have been a number of computational studies dedicated to spin crossover compounds using the density functional theory (DFT)[20-28] as well as higher levels of theory, such as CASPT2 (complete active space with second-order perturbation theory).[29-30] Due to the size of these systems (50 or more atoms), they are most amenable to calculations performed by the DFT methods. While DFT is very successful at predicting geometries of both high-spin and low-spin complexes,[19] obtaining the correct ground state represents a major challenge since GGA (generalized gradient approximation) functionals (e.g., PBE) tend to favor the low spin states, while the hybrid functionals (e.g., B3LYP) artificially favor the high spin states. Reiher and coworkers related this behavior to the amount of exact Hartree-Fock exchange used in the hybrid functionals.[25] While it is difficult to accurately determine the ground state of spin crossover complexes or the exact energy differences between their high-spin and low-spin states with the DFT methods, it is at least possible to qualitatively predict the effect of ligand substitution on the spin transition behavior.[20, 23-24]

The objectives of this work are to: (1) ***evaluate DFT*** as a tool for calculations of Fe(II) complexes in their function of photosensitizers, (2) ***obtain a better understanding of the experimental findings*** on Fe(II) complexes investigated as photosensitizers and published in the literature.[3-8]

The description of our results is organized into two parts as follows: First, we summarize our results on the applicability of the B3LYP functional to the ground state determination of pseudo-octahedral iron complexes, with special focus on Fe(II)-polypyridines. We explore systematic trends in the calculated energy differences between the high-spin and low-spin electronic states for a series of experimentally known transition metal complexes. Finally, we suggest that the ground state of an arbitrary Fe(II) complexes can be determined by comparing the calculated energy difference between the low-spin

and high-spin electronic states to the energy differences of structurally related complexes with a known, experimentally-determined ground state, without the need to reparametrize the functional.

Second, we describe our studies on the light absorption and IET processes for three different dye-TiO_2 nanoparticle systems, with a special focus on elucidating the origin of the band-selective IET in Fe(II) polypyridine-TiO_2 assemblies. The dyes investigated include $[Fe(bpy)(CN)_4]^{2-}$ (**1**), $[Fe(bpy\text{-}dca)(CN)_4]^{2-}$ (**2**), and $[Fe(bpy\text{-}dca)_2(CN)_2]$ (**3**), shown in Figure 1. Two of these dyes were studied previously, **1** by Meyer[14-15] and **3** Ferrere.[11, 13] While **3** attaches to the TiO_2 surface via the carboxylic acid anchoring group, **1** is attached via the CN^--Ti bridge. Although dye **2** was not studied experimentally, it represents a natural bridge between the complexes **1** and **3** and was therefore included in our computational study.

5. Summary of the most important results

5.1. Benchmarking the DFT methodology

5.1.1 Computational Approach

Twenty seven pseudo-octahedral complexes of Fe, Co, Mn, Ru and Os with a mixture of heteropyridine and Cl^-, F^-, CN^-, NCS^-, and H_2O ligands were investigated. The majority of the complexes (19) are complexes of iron. Heteropyridine ligands considered are shown in Figure 2. They include bpy = 2,2'-bipyridine, phen = 1,10-phenanthroline, terpy = 2,2';6',2"-terpyridine, $tren(py)_3$ = tris((N-(2-pyridylmethyl)-2-iminoethyl)amine), $tren(6\text{-}Me\text{-}py)_3$ = tris((N-(2-(6-Me-pyridyl)methyl)-2-iminoethyl)amine), Lt = 4-(4-bromophenyl)-2,6-bis(2-pyridine)-1,3,5-triazine, Me-Lt = 4-(4-bromophenyl)-2,6-bis(6-picolinyl)-1,3,5-triazine, tpen = tetrakis(2-pyridylmethyl)ethylenediamine, and (pyrol)3tren = tris(1-(2-azoyl)-2-azabuten-4-yl)amine ligands.

Geometries of all compounds were initially optimized at the B3LYP level of theory.[31] SDD relativistic effective core potential and associated triple-ζ basis set[32] was used to describe the metal center and 6-311+G* basis set[33-34] was used for all other atoms. Singlet and quintet states were optimized for complexes of Fe(II), Co(III), Ru(II), and Os(II), doublet and sextet states were optimized for complexes of Fe(III) and Co(II), triplet and quintet states were optimized for the Mn(III) complex.

To investigate the dependence of high-spin vs. low-spin energy differences ($\Delta E_{HS/LS} = E_{high-spin} - E_{low-spin}$, $\Delta H_{HS/LS} = H_{high-spin} - H_{low-spin}$, $\Delta G_{HS/LS} = G_{high-spin} - G_{low-spin}$) on the amount of exact exchange in the B3LYP functional, we have systematically varied c_1 parameter from 0.0 to 0.25, corresponding to 0-25% Hartree-Fock exchange in the exchange-correlation functional of B3LYP:

$$E_{xc} = E_{xc}^{LSDA} + c_1(E_x^{exact} - E_x^{LSDA}) + c_2\Delta E_x^{B88} + c_3\Delta E_C^{PW91} \quad \mathrm{E_{xc}} = \mathrm{E_{xc}^{LSDA}} + \mathrm{c_1}\left(\mathrm{E_x^{exact}} - \mathrm{E_x^{LSDA}}\right) + \mathrm{c_2}\Delta\mathrm{E_x^{B88}} + \mathrm{c_3}\Delta\mathrm{E_C^{PW91}}, \qquad (1)$$

in which c_1, c_2, and c_3 are coefficients fit from experimental data (determined to be $c_1 = 0.20$, $c_2 = 0.72$, $c_3 = 0.81$),[31] $\mathrm{E_{xc}^{LSDA}}$ is the exchange-correlation energy from the local spin density approximation (LSDA),[35] E_x^{exact} is the exact exchange energy, E_x^{B88} is Becke's 1988 gradient correction of exchange,[36] and ΔE_C^{PW91} is Perdew and Wang's 1991 gradient correction to correlation.[37]

The low spin and high spin geometries of all compounds were fully re-optimized for each different value of the exact exchange in the B3LYP functional. All optimized structures were verified using vibrational frequency analysis. The results of vibrational analysis were used to obtain enthalpies (*H*) and free energies (*G*) for all compounds at 298.15 K. An ultra-fine integration grid was used for all calculations.

Calculated expectation values of the S^2 operator are within 10% of the value expected for each complex, except for the doublet spin-state of $[FeF_6]^{3-}$ ($< S^2 > = 1.79$ in vacuum and $< S^2 > = 1.14$ in water) and $[FeCl_6]^{3-}$ ($< S^2 > = 1.67$ in vacuum and $< S^2 > = 1.30$ in water). The resulting wavefunctions were also tested for stability.[38-39] All species were optimized in vacuum and solvent (water) using Polarizable Continuum Model (PCM), with the exception of $[Fe(Me\text{-}Lt)_2]^{2+}$ which was relaxed in vacuum only.[40] The use of solvent improved the structures and spin contamination of anionic compounds, while it did not have

any significant influence on optimized geometries of cations and neutral species. All calculations were performed using Gaussian 09 software package.[41]

5.1.2. Results and Discussion

Ground state determination by B3LYP, energies of high-spin vs. low-spin states. While B3LYP can be used as a reliable tool in obtaining high-spin and low-spin geometries of first row transition metal complexes, it is not as reliable in predicting their ground state spin multiplicity. Out of the 25 first row transition metal complexes investigated, B3LYP was incorrect in predicting the ground state of eight of these, artificially favoring the high-spin state over the low-spin state in seven of the cases (see Table 1). Inclusion of thermal and entropic factors further stabilized high-spin state in four more complexes and incorrectly predicted the high-spin ground state for 10 of the 25 complexes. Such bias toward the high-spin states is not unusual for the B3LYP and has been observed before.[26]

Following the example of Reiher et al.,[26] we have calculated the energy ($\Delta E_{HS/LS}$), as well as enthalpy ($\Delta H_{HS/LS}$) and free energy differences ($\Delta G_{HS/LS}$) between the high-spin and low-spin states for a group of transition metal compounds with respect to the exact exchange admixture in the B3LYP functional form (c_1 = 0.00 - 0.25, see Equation 1). The energy difference was defined as $\Delta E_{HS/LS} = E_{high-spin} - E_{low-spin}$ ($\Delta H_{HS/LS} = H_{high-spin} - H_{low-spin}$, $\Delta G_{HS/LS} = G_{high-spin} - G_{low-spin}$) and is positive if the low-spin state is calculated to be more stable than the high-spin state.

Figure 3 shows the $\Delta E_{HS/LS}$ dependence on c_1 for a number of different Fe(II) pseudo-octahedral complexes with polypyridine as well as non-polypyridine ligands. While $\Delta E_{HS/LS}$ depends linearly on c_1, the slope of this dependence varies widely among the complexes and it is not possible to fit this dependence with a single linear equation for all complexes investigated. Similar behavior has been reported previously by Salomon et al.[27] for a different set of first row transition metal complexes. Interestingly, $[FeF_6]^{3-}$ displays nonlinear behavior in its dependence of $\Delta E_{HS/LS}$ on c_1 when optimizations are performed in vacuum. Further investigation of this phenomenon revealed the presence of two different high-spin states for this complex, whose relative stabilities change depending on the amount of exact exchange in the B3LYP functional. Therefore, calculations performed with lower admixture of exact exchange converge to a different electronic state than those with a higher admixture, resulting in the nonlinear behavior. This problem of state switching for $[Fe(F)_6]^{3-}$ is not present when optimizations are performed in solvent (H_2O) using PCM.

Table 2 summarizes the behavior of all complexes investigated, giving the slope of the linear fit for the dependence of $\Delta E_{HS/LS}$, $\Delta H_{HS/LS}$, and $\Delta G_{HS/LS}$ on the amount of exact exchange (c_1). Interestingly, all Fe(II)-polypyridine complexes have similar slope of ΔE vs. c_1 across the 0.0 – 0.25 range of the exact exchange admixture. On the other hand, while the dependence of ΔE vs. c_1 for more ionic complexes (e.g., $[Fe(H_2O)]^{2+}$, $[FeCl_6]^{4-}$) is still linear, the slope of this dependence is completely different from that of the Fe(II)-polypyridine compounds. This makes it challenging to come up with a single correction scheme for a wide variety of transition metal compounds. We suggest that there is a connection between the slope of the ΔE vs. c_1 dependence and structural features of the complexes, as well as the character of metal-ligand bonds in the complex (ionic vs. covalent).

Structure of Fe(II) complexes and error in high-spin/low-spin energies from B3LYP. According to the ligand field theory, the ligand field splitting between a set of t_{2g} and e_g metal orbitals is determined by the identity of a central atom and its ligands. The size of the ligand field splitting determines the ground state electronic configuration (high-spin vs. low-spin) as well as the energy difference between the high-spin/low-spin states of a particular octahedral compound. Therefore, it would not be surprising if there were some link between the structure of the complexes investigated and the slope of $\Delta E_{HS/LS}$ vs. c_1.

The change in the electronic configuration from high-spin to low-spin and vice versa is usually accompanied by a marked change in the metal-ligand bond lengths of the covalent complexes, as placing the electrons into the antibonding e_g orbitals increases the metal-ligand distance in the high-spin state. Therefore, we have explored the relationship between the average change in the metal-ligand distance

(ΔR) and the slope of the $\Delta E_{HS/LS}$ dependence on amount of exact exchange in the B3LYP functional (c_1). The reported ΔR is an average over the c_1 range investigated, but the results are virtually identical when only considering ΔR calculated at $c_1 = 0.2$ (unmodified B3LYP functional).

Table 2 summarizes the average change in the metal-ligand distance between the high-spin and low-spin state determined at the B3LYP level of theory along with the slope of the $\Delta E_{HS/LS}$, $\Delta H_{HS/LS}$, and $\Delta G_{HS/LS}$ dependence on c_1. The change in the metal-ligand distance was determined as an average of the changes calculated for all values of c_1 investigated between 0.0 and 0.25. Figure 4 shows the plot of the average change in the metal-ligand bond lengths between the high-spin and low-spin states, with respect to the slope of the $\Delta E_{HS/LS}$ vs. c_1 dependence. Interestingly, there is a linear relationship between the two, showing that a smaller slope corresponds to a smaller change in the bond lengths. The R^2 coefficient for this dependence is 0.93, suggesting a strong correlation. Second and third-row transition metal compounds ($[Ru(bpy)_3]^{2+}$, $[Os(bpy)_3]^{2+}$, shown in blue) were excluded from the fit, but are still shown on the plot. A weaker correlation is observed, with an R^2 value of 0.78, when all species are optimized in vacuum. All species reported in Table 2 were optimized using PCM solvent model for H_2O excluding $[Fe(Me\text{-}Lt)_2]^{2+}$, which was optimized in vacuum.

It is apparent that the complexes with the weakest dependence of $\Delta E_{HS/LS}$ on c_1 are ionic compounds of first row transition metals (e.g., $[Fe(H_2O)_6]^{2+}$, $[FeCl_6]^{3-}$) that also undergo smallest change in the metal-ligand bond lengths between the low spin and high spin states. Complexes with more covalent character of metal-ligand bonds undergo larger structural changes between their low-spin and high-spin electronic states and are more strongly influences by the amount of exact exchange admixture in the DFT functional.

The outliers to this trend are shown in blue and belong to octahedral compounds with a central atom from second and third row of transition metals (Ru and Os), suggesting that the relationship between the average change in metal-ligand bond lengths and the slope of the $\Delta E_{HS/LS}$ dependence on c_1 will have a different character than displayed by the complexes of first row transition metals.

Note that a similar relationship as observed between the dependence of $\Delta E_{HS/LS}$ on c_1 vs. ΔR holds true for $\Delta H_{HS/LS}$ and $\Delta G_{HS/LS}$. However, the correlation for this dependence becomes slightly worse with the thermal and entropic corrections included ($R^2 = 0.93$ and 0.91, respectively). This is not very surprising, as several assumptions are made in obtaining these corrections (i.e., assumption of harmonic potential, neglecting the role of the solvent) that are not equally good for all compounds investigated in this study. The problem is exacerbated by the fact that the low frequency vibrations, which provide the largest contribution to the entropy, suffer from the highest error in the harmonic approximation.[25]

It is also worth mentioning that identical results are obtained when the analysis is performed with a smaller basis set (6-31G* instead of 6-311+G*) and in vacuum. The larger basis set and solvent model are, however, necessary in order to obtain proper description of the structures and electronic states of some anionic compounds (e.g. $[Fe(CN)_6]^{4-}$, $[FeF_6]^{3-}$).

Ground state determination for a family of structurally related complexes. The linear correlation between the average ΔR and slope of the $\Delta E_{HS/LS}$ vs. c_1, suggests that the octahedral complexes that undergo similar distortion in their octahedral environment going from a low-spin to high-spin state (described here by the average change in metal-ligand bond lengths), suffer from the similar error in the B3LYP functional. In case of the covalent complexes of iron, this systematic error results in the artificial stabilization of their high-spin state energies with respect to the low-spin state energies. The question still remains if this error is systematic for a group of similar complexes, i.e. if it results in the artificial stabilization of the high-spin state energies with respect to the low-spin state energies by about the same amount.

To find if the error is indeed systematic, we have looked at the $\Delta E_{HS/LS}$ vs. c_1 dependence in a set of ten structurally-related Fe(II)-polypyridine complexes. They were chosen as "structurally-related" because they display similar geometry change in the metal-ligand bond lengths going from low spin to high spin geometry (see Table 2). The selected complexes contain polypyridine ligands combined with other ligands

of varying ligand-field strength, such as Cl^-, NCS^-, and CN^-. The plot of the $\Delta E_{HS/LS}$ as a function of c_1 for six members from this family of related Fe(II) compounds is shown in Figure 5.

As can be seen in Figure 5, the dependence of $\Delta E_{HS/LS}$ on c_1 is linear, with approximately the same slope for the compounds considered. Note that very similar linear dependence of $\Delta E_{HS/LS}$ on c_1 as well as systematic errors for a group of related Fe(II)-S complexes have been observed previously by Reiher and coworkers.[26] In case of our Fe(II) test complexes, this linear relationship between ΔE and c_1 can be described by the following equation:

$$\Delta E_{HS/LS} = I - 142.5 c_1 \quad \Delta E_{HS/LS} = I\text{-}140.2 c_1, \qquad (2)$$

where I corresponds to the intercept (the value of $\Delta E_{HS/LS}$ at $c_1 = 0$ for each complex) which describes the vertical shift between the plots of $\Delta E_{HS/LS}$ vs. c_1 for different complexes. The four complexes included in the fit but not shown in Figure 5 are: $[Fe(Lt)_2]^{2+}$, $[Fe(Me\text{-}Lt)_2]^{2+}$, $[Fe(phen)_3]^{2+}$, $[Fe(terpy)_2]^{2+}$, and $[Fe(tpen)]^{2+}$. The above equation fits the $\Delta E_{HS/LS}$ dependence on c_1 for each of the eleven complexes very accurately, with the correlation coefficient R^2 = 0.97-0.99. More importantly, the vertical shift between plots of $\Delta E_{HS/LS}$ for different Fe(II) compounds correctly reflects the change in the ligand field strength of their ligands, meaning that the low-spin states of Fe(II) compounds are stabilized over the high-spin states in the same order as the Fe(II) ligands appear in the spectrochemical series: $Cl^- < NCS^-$ < pyridine < bipyridine < CN^-. This means that although B3LYP is not capable to predict the correct ground state spin multiplicities, the overall order of the high-spin/low-spin energy differences for a group of structurally related compounds reflects their high-spin, low-spin, or thermal spin crossover character in the ground state.

It should be noted that when comparing $[Fe(phen)_3]^{2+}$ and $[Fe(bpy)_3]^{2+}$ we found that the trend in $\Delta E_{HS/LS}$ vs. c_1 incorrectly reflected the trend in ligand field strength, however the distance between the two plots of $\Delta E_{HS/LS}$ over c_1 = 0-0.25 were at most 2.0 kcal/mol. $[Fe(phen)_3]^{2+}$ is not shown in Figure 5, but belongs to the same set of structurally-related complexes. Phen and bpy ligands are considered to have very similar ligand field strength, so this discrepancy is well within the accepted error range for the B3LYP functional.

The linear behavior of $\Delta E_{HS/LS}$ with respect to c_1, along with the systematic trend in the intercept I for a series of related compounds, can therefore be used to construct a benchmark for determination of the ground state multiplicity for an arbitrary Fe(II)-polypyridine complex. A procedure to determine the ground state multiplicity of an arbitrary Fe(II)-polypyridine complex could be as follows: (1) Obtain $\Delta E_{HS/LS}$ vs. exact exchange dependence plots for a series of related compounds with available experimental reference data. (2) Based on this benchmark, decide which values of the intercept I correspond to the high-spin and low-spin ground states. In the specific example of Fe(II)-polypiridines shown in Figure 5, I > 24 kcal/mol indicates a low-spin complex, I < 18 kcal/mol high-spin complex, with I = 18-24 kcal/mol indicating a possible thermal spin crossover complex. (3) Obtain $\Delta E_{HS/LS}$ vs. exact exchange dependence plot for the compound with unknown ground state. (4) Based on the intercept I obtained for the unknown compound, determine its spin state.

For a series of related complexes this procedure will produce a unique range of I values for low-spin and high-spin stability. A questionable spin crossover region will also always exist between the two stability regions due to inherent error in the method. The value of I for a thermal spin crossover complex determines where the low-spin and high-spin states change relative stability. The average of the intercepts for the two thermal spin crossover complexes ($[Fe(tpen)]^{2+}$, $[Fe(bpy)_2(NCS)_2]^0$) is 21 kcal/mol which is, interestingly, close to the determinded exchange interaction between electrons in the d orbitals of iron.[42-44] We believe this is a coincidence since the intercept for a spin crossover complex represents the error in $\Delta E_{HS/LS}$ when the B3LYP functional is reparameterized to be a purely GGA functional (c_1=0), which still contains exchange interaction.

The strong linear correlation between the average ΔR and slope of the $\Delta E_{HS/LS}$ vs. c_1 scans could also allow us to forgo the calculation of $\Delta E_{HS/LS}$ vs. c_1 dependence for several values of c_1 for both benchmark and unknown complexes. It makes it possible for us to rely on the average change in the octahedral coordination environment to determine what group of complexes is "similar" for the purposes

of the ground state determination and reduces the number of calculations one needs to perform to just B3LYP with a single value of $c_1 = 0.2$. Analogous analysis with virtually identical results toward lower energies can also be performed using $\Delta H_{HS/LS}$ or $\Delta G_{HS/LS}$ instead of $\Delta E_{HS/LS}$, noting that the calculated $\Delta H_{HS/LS}$ and $\Delta G_{HS/LS}$ will be systematically shifted toward lower energies.

5.2. Elucidating band-selective injection

5.2.1 Computational Approach

Molecular Structure and Absorption Spectra. Dye molecules were optimized at the B3LYP[31, 45] level of theory. The SDD relativistic effective core potential (ECP) and associated basis set[32] were used to describe the central iron atom, and 6-31G* basis sets[33-34] were used for all other atoms. All complexes were optimized in the singlet ground state in vacuum. The calculation of UV-vis absorption spectra for dyes **1-3** was performed employing TD-DFT[46-48] methodology with the same basis set and functional as used for the geometry optimizations. Only spin allowed singlet vertical excitations were determined and TD-DFT was performed on the entirely relaxed dye molecules **1-3**. Polarizable continuum model (PCM)[49], using acetonitrile as a solvent, was employed in the TD-DFT calculations. Absorption spectra were simulated by convoluting the stick spectrum composed of the δ-functions associated with each excitation energy times the oscillator strength with a Lorentzian line shape with half-width-at-half-maximum (HWHM) of 0.12 eV. Canonical Kohn-Sham orbitals were used to characterize absorption peaks with $f_{osc} > 0.01$, within the visible portion of the spectra ($\lambda > 350$ nm). The Gaussian 09 software package[41] was used for all the DFT and TD-DFT calculations on dye molecules.

Slab Model Optimization. The Vienna Ab-initio Simulation Package (VASP)[50-53] was used to optimize periodic systems (bulk TiO_2 and nanoparticles) at DFT level of theory. The Perdew-Burke-Ernzerhof (PBE)[54-55] exchange-correlation functional with Projector Augmented-Wave method[56-57] was employed in all periodic boundary calculations (PBCs). The plane wave basis set expansion was cutoff at 500 eV for all PBCs. The unit cell for anatase TiO_2 was obtained with a (13 x 13 x 13) *k*-point sampling, resulting in a tetragonal lattice with lattice vectors $a = b = 3.81$ Å, $c = 9.77$ Å). The optimized geometry of the TiO_2 unit cell was used to construct a slab model of the (101) TiO_2 surface functionalized with either hydrogen cyanide or pyridine-4-carboxylic acid. The linker models and the top 2 layers of Ti and top 4 layers of O were relaxed using a (5 x 3 x 1) *k*-point sampling, keeping the supercell volume fixed with lattice vectors $a = 15.25$ Å, $b = 10.49$ Å, $c = 26.00$ Å. The bottom layers of the slab were fixed at bulk geometry.

The final model dye-nanoparticle assemblies were constructed by performing a constrained optimization of the dyes **1-3** with the linker groups (cyanide, and carboxylic acid in both monodentate and bidentate surface binding modes) fixed at surface-optimized geometries. Coordinates for the carboxylate functional group as well as the three closest carbons in the pyridine ring along with the two adjacent hydrogens were held frozen in the constrained optimization of dyes **2** and **3**. The Gaussian 09 software package,[41] employing the same functional and basis sets as above, was used for these constrained optimizations of dye with frozen linker geometry. Dyes **2** and **3** were attached to the slab surface in a cyanide, monodentate carboxylic acid, and bidentate carboxylate binding modes via the Kabsch alignment.[58] Dye **1** was attached in the same manner with a cyanide binding mode. All the nonequivalent linker positions on the dyes were modeled: two nonequivalent carboxylic acid groups on **1** and **2** and two nonequivalent cyanide groups on **3**. All optimizations were performed in vacuum.

Interfacial Electron Transfer Simulations. All model systems were composed of a (101) anatase nanoparticle slab with dyes (**1-3**) attached via an anchoring group (cyanide or carboxylic acid) in vacuum and their construction is described above. Quantum dynamics simulations to model the interfacial electron transfer (IET) were performed on each dye-semiconductor model using a method developed by Rego and Batista,[59] employing the extended Hückel (EH) Hamiltonian. Details of this method can be found in references 59 and 60. Survival probability was obtained at each simulation step by projecting of the time-evolved wave function onto the atomic orbitals of the adsorbed chromophore. Characteristic electron injection time was then obtained from an exponential fit of the survival probability.

For each system, donor states in the IET simulations were chosen from the particle states that make up major contributions to prominent excitations in the visible region of the absorption spectrum (f_{osc} > 0.01, λ > 350 nm) as calculated by TD-DFT calculations. The canonical Kohn-Sham orbitals corresponding to the relevant particle states were matched to the EH orbitals.

Simulations were run with a time step of 0.1 fs up to 3000 fs on super-cell arrays with 30.49 Å × 31.46 Å × 26.00 Å dimensions. One *k*-point was used for sampling and the calculation was run using periodic boundary conditions. All simulations were done at the frozen geometry. Absorbing potentials (i.e., imaginary terms to the diagonal elements of the Hamiltonian) were placed on the bottom layer of Ti atoms to avoid artificial recurrences in the electron-transient populations.

The survival probability curves were fit with either a exponential decay function, or in the case that $R^2 < 0.95$, a biexponential decay function. The survival probability was constrained to unity at time 0 for all fits. The characteristic injection time was determined by the reciprocal of the decay constant for single exponential functions, or the reciprocal of the decay constant responsible for the majority of decay (coefficient > 0.50) for the biexponential functions.

5.2.2. Results and Discussion

The results are organized as follows: First the ground state molecular properties and absorption spectra are described for all dyes, followed by the description of the dye-nanoparticle assemblies. Finally, results of the IET simulation are summarized for each dye individually.

Ground State Structures and Absorption Spectra. The optimized structures of dyes **1 - 3** are shown in Figure 6. Metal-ligand bond lengths for all three complexes are reported in Table 3, using the atom-numbering scheme from Figure 6. For dye **1**, we find a 2% error when comparing B3LYP metal-ligand bond length to the experimental crystal structure data.[61] For dye **2**, crystal structure data is unavailable but we assume errors are similar to the related dye **1**. For dye **3**, crystal structure data is only available for the related species $[Fe(bpy)_2(CN)_2]$. When comparing the metal-ligand bond lengths for the singlet state of dye **3** to the corresponding bonds from the crystal structure of $[Fe(bpy)_2(CN)_2]$, we find only a 2% error.[62] Overall, B3LYP provides accurate geometries for all the dyes.

The simulated absorption spectra for dyes **1**-**3** are shown in Figure 7. All three complexes display two absorption bands in the visible region. Excitations A-C (complex **1**) and A-F (complex **2**) can be all described as metal-to-ligand charge transfer (MLCT) transitions. While majority of the transitions A-J (complex **3**) also have a MLCT character, several transitions (D, E) have significant metal-centered (MC) character.

Relevant particle states involved in the visible light transitions are shown in Figure 8, classified by the absorption band. Note that functionalization of the bipyridine ligand of dye **1** with dicarboxylic acid, resulting in dye **2**, changes the energetic ordering of the LUMO+1 and LUMO+2 orbitals. Complex **3** possesses three degenerate sets of virtual orbitals (LUMO, LUMO+1 and LUMO+2, LUMO+3) and a contribution from metal-centered ligand field state (LUMO+12). The particle states shown in Figure 8 serve as initial (donor) states for the IET simulations reported below.

Dye-Nanoparticle Assemblies. The linker models used to attach the dye molecules to the TiO_2 surface are shown in Figure 9. We have explored cyanide attachment mode, and monodentate and bidentate attachment modes for carboxylic acid. Although multiple carboxylic acid binding modes exist, only two attachment modes are explored in this work, based on previously published stability analysis.[63]

Each of the Fe(II) polypyridine compounds investigated can attach to the surface in multiple ways. Complex **3** can be anchored to the TiO_2 surface via –COOH group attached at 4 or 4' site of the bpy ligand. Similarly, two non-equivalent CN^- sites for attachment are present in **1** and **2**. This results in two possible attachments of all three dyes onto the surface, in which the bipyridine group not bound to the surface is oriented either parallel or perpendicular relative to the (101) plane of TiO_2 (see Figure 10).

Dyes anchored to the surface via the CN^- group have a free degree of rotation about the axis defined by the cyanide bond (see Figure 11). This ambiguity is caused by the fact that HCN-TiO_2 surface

model was chosen to model the full dye-TiO_2 assembly due to the computational constrains. A conformation that places the bipyridine groups as far from the surface as possible was chosen for the IET simulations reported here. This allows us to study the IET via the surface-anchoring group, rather than indirect IET between the bpy ligand group and TiO_2 surface due to their spatial proximity.

It is important to note that the structure optimization of the HCN/TiO_2 system (see Figure 11) resulted in a significantly longer N-Ti bond length (2.33 Å) than that reported by Selloni[64] (2.12 Å). Selloni and coworkers have optimized $[Fe(CN)_6]^{4-}$ on a $Ti_{38}O_{76}$ cluster, which likely provides a better model for this attachment. The influence of the N-Ti distance on the results on the IET rates was therefore investigated by setting the N-Ti bond length to 2.12, 2.22, and 2.33 Å in the IET simulations as shown in Figure 11.

Interfacial Electron Transfer Simulations. Density of states plots for chromophore-nanoparticle assemblies calculated with the extended Hückel method are shown in Figures 12 and 13. For all three complexes investigated, dyes introduce occupied energy levels into the semiconductor band gap and a number of virtual energy levels (LUMO – LUMO + 12 for dye **1**, LUMO – LUMO + 13 for dye **2**, and LUMO – LUMO + 15 for dye **3**) that couple with the conduction band of TiO_2.

Differences in the orbital energy levels among the three dyes are illustrated in Figure 13. Addition of carboxylic acid groups to bipyridine ligand of dye **1** creating dye **2**, results in the significant lowering of the orbital energies of LUMO – LUMO+2 states. Replacement of the two CN^- ligands in dye **2** by an additional bipyridine ligand creating dye **3** results in a set of three of doubly degenerate virtual orbitals (LUMO – LUMO+5).

Results of the IET simulations are summarized in Figures 14-16. In order for the IET to be competitive with the ultrafast intersystem crossing into a low-lying ^5T state in these complexes, the IET characteristic time, τ, should be smaller or equal to 100 fs.[18, 20, 21] A horizontal red line in Figures 14-16 denotes the characteristic time τ = 100 fs. Therefore, only the initial states with this or faster rates (i.e., lying below the red line) will be capable of the electron injection into the TiO_2 semiconductor.

As can be seen in Figure 14, excited dye **1** will not undergo IET efficiently, as the majority of the characteristic times are between 483.0 fs – 17.7 ps. The only exception is the IET from LUMO+1 orbital in the bpy perpendicular attachment. In the LUMO+1 case the characteristic times range between 137.3 – 101.6 fs, suggesting that while the IET is not very efficient in **1**-TiO_2 assemblies, it does occur for certain excitations. This is consistent with the work of Meyer[14] which indicates that the excited state charge transfer in **1**-TiO_2 assemblies occurs via a combination of the direct sensitization mechanism (i.e., direct charge-transfer excitation between the dye and the semiconductor) as well as the indirect mechanism (i.e., IET). It is also interesting to note that the IET is overall more efficient when the plane defined by the single bipyridine ligand is oriented perpendicular with respect to the TiO_2 surface. Additionally, variation of the CN^- group distance from the TiO_2 surface between 2.12 – 2.33 Å does not significantly impact the calculated IET rates. Therefore, only Ti-N distance of 2.33 Å was considered in all subsequent IET simulations.

Figure 15 summarizes the IET rates for **2**-TiO_2 assemblies. Both bidentate and monodentate attachments via the carboxylic acid anchoring group were investigated, as well as the attachment via the CN^- ligand. There are several conclusions that can be drawn from these results. First, IET via the CN^- ligand for **2**-TiO_2 assemblies is much less efficient than in the case of the **1**-TiO_2. This is likely due to the stabilization of the MLCT states localized on the bpy ligand caused by addition of the carboxylic acid groups (see Figure 13). As a result, IET via the CN^- anchoring group will not be competitive with the ultrafast intersystem crossing events in these complexes. Second, this complex displays a band-selective IET when attached to the TiO_2 via the carboxylic acid anchoring group in both monodentate and bidentate binding modes. Interestingly, IET via the monodentate binding mode is overall more efficient than via the bindentate binding mode. Finally, comparison of the IET characteristic times among **1**-TiO_2 and **2**-TiO_2 leads us to conclude that indirect sensitization will be more efficient in **2**-TiO_2 thanks to the presence of the carboxylic acid anchoring groups. On the other hand, attachment of this complex via the carboxylic acid group will eliminate the direct sensitization mechanism that occurs when the complex is attached to TiO_2 via the CN^- group.[14]

Characteristic IET times for **3**-TiO_2 assemblies are shown in Figure 16. As can be seen in Figure 16, dye **3** undergoes a band-selective IET for all attachments investigated. Interestingly, attachment via the carboxylic acid anchoring group in monodentate binding modes results in the fastest IET rates on average. Note that while LUMO – LUMO+4 belong to the π^* ligand-localized states, LUMO+15 (which matches Kohn-Sham orbital LUMO+12) corresponds to a metal-centered state (see Figure 8). This accounts for an ultrafast IET from this state (τ = 12.4 fs) for CN^- attachment, while significantly slower IET rates (τ = 302.9 fs – 7.3 ps) were observed for the **3**-TiO_2 assemblies employing carboxylic acid as the anchoring group.

Interestingly, band-selective sensitization was observed in dye-TiO_2 assemblies for all three dyes investigated. While our results do not elucidate this phenomenon for the **1**-TiO_2 system, they do provide an explanation in case of the **2**-TiO_2 and **3**-TiO_2 assemblies. Band 1 (the lowest energy band in the UV-vis spectrum) corresponds to the excitations into the LUMO of **2** and a nearly degenerate set of LUMO and LUMO+1 orbitals of **3** (see Figures 7 and 8). These orbitals lie at the edge of the TiO_2 conduction band (see Figure 13) where the density of TiO_2 states is low, which results (1) into a small number of TiO_2 acceptor states available to couple with the donor states (LUMO, LUMO+1) of **2** and **3** and (2) small driving force for the IET. Our results are consistent with the experimental observations of Ferrere and coworkes who first identified this band-selective behavior in **3**-TiO_2 assemblies.[13] Moreover, they also provide a pathway to improving the efficiency of these chromophores: In order to improve the IET efficiency, one needs to increase the energy of the LUMO and LUMO+1 states which should increase the driving force for the electron injection as well as provide a larger number of the TiO_2 acceptor states capable of coupling with the dye donor states.

6. Conclusion

In this work, we investigated the applicability of the B3LYP functional to accurate prediction of ground state multiplicity of pseudo-octahedral iron complexes. Iron complexes are of great interest due to potential applications as molecular switches, data storage materials, and chromophores in dye-sensitized solar cells. Their properties intrinsically depend on their ground state, which, depending on the ligand character, can be either low-spin or high-spin. In general, density functional theory has difficulties with predicting the correct ground state multiplicity of such compounds, as pure functionals favor the low-spin states and hybrid functionals with high fraction of exact Hartree-Fock exchange tend to favor high-spin ground states.

We confirmed the linear relationship between the high-spin/low-spin energy splitting, $\Delta E_{HS/LS}$ ($\Delta E_{HS/LS} = E_{high\text{-}spin} - E_{low\text{-}spin}$), as well as $\Delta H_{HS/LS}$ and $\Delta G_{HS/LS}$, and the amount of exact exchange in the B3LYP functional as previously observed by Reiher and coworkers.[25] For coordination complexes of iron with mostly covalent character, such as Fe(II)-polypyridines, $\Delta E_{HS/LS}$ displays a strong dependence on the amount of exact exchange in the functional and B3LYP tends to favor high-spin ground states. On the other hand, $\Delta E_{HS/LS}$ for ionic complexes displays a weaker dependence on c_1, and B3LYP artificially stabilizes the low-spin states.

We confirmed that in most cases investigated, dependence of $\Delta E_{HS/LS}$ on c_1 is linear over the range of 0-25% of exact exchange admixture in B3LYP. We found that the slope of this dependence strongly correlates with the average change in the metal-ligand bond lengths between the low-spin and high-spin states. Moreover, the error in $\Delta E_{HS/LS}$ for a group of structurally related complexes (i.e., complexes that undergo similar change in the metal-ligand bond lengths between the high-spin and low-spin states) is systematic and the calculated values of $\Delta E_{HS/LS}$ correctly reflect the trend in the relative stabilities of their low-spin and high-spin states. Inclusion of thermal and entropic corrections tends to stabilize the high-spin states, but nevertheless results in the identical behavior. **This systematic behavior allows for a ground state determination of an arbitrary pseudo-octahedral complex of iron by comparing the calculated energy differences between the singlet and quintet electronic states of an unknown complex to the**

energy differences of structurally related complexes with a known, experimentally determined ground state.

We have, furthermore, studied initial excitation and subsequent IET among three Fe(II)-polypyridine dyes and TiO_2 anatase semiconductor. We find that all three complexes investigated can undergo IET at the time scale competitive with the ultrafast intersystem crossing of the initially excited ^{1}MLCT states into the low-lying metal-centered states of higher multiplicities. The sensitization is more efficient when the dyes are attached to surface via the carboxylic acid anchoring group rather than CN^-. Attachment via the carboxylic acid in a monodentate binding mode also results in more efficient IET rates in comparison to the bidentate attachment.

All three complexes investigated display band-selective sensitization, which is consistent with previous experimental findings by Ferrere and coworkers.[11, 13] **The origin of the band-selective behavior is attributed to the poor alignment of the lowest energy excited states with the conduction band of the TiO_2 semiconductor.** This results in a poor driving force for the injection and insufficient density of the semiconductor acceptor states available for coupling with the dye donor states. One way to improve the efficiency of Fe(II)-polypyridine based dyes would be to increase the energy of their LUMO and LUMO+1 states with respect to the conduction band of the semiconductor. This could be, for example, achieved by targeted functionalization of their polypyridine scaffolds by electron donating groups.

In conclusion, we have shown that DFT is a valid tool that can be employed in computational studies of Fe-based coordination compounds. DFT, TD-DFT, and quantum dynamics simulations were also successful in describing and elucidating the band-selective IET behavior in Fe(II)-polypyridine-TiO_2 nanoparticle assemblies.

7. Bibliography

1. Ardo, S.; Meyer, G. J., Photodriven Heterogeneous Charge Transfer with Transition-Metal Compounds Anchored to TiO_2 Semiconductor Surfaces. *Chem. Soc. Rev.* **2009,** *38*, 115.
2. Sakaki, S.; Kuroki, T.; Hamada, T., Synthesis of a New Copper(I) Complex, $[Cu(tmdcbpy)_2]^+$ (tmdcbpy = 4,4,6,6-Tetramethyl-2,2-Bipyridine-5,5-Dicarboxylic Acid), and its Application to Solar Cells. *Dalton Trans.* **2002**, 840.
3. Ferrere, S., New Photosensitizers Based Upon [Feii(L)2(Cn)2] and [Feiil3], Where L is Substituted 2,2'-bipyridine. *Inorg. Chim. Acta* **2002,** *329*, 79.
4. Yang, M.; Thompson, D. W.; Meyer, G. J., Dual Pathways for TiO_2 Sensitization by $Na_2[Fe(bpy)(CN)_4]$. *Inorg. Chem.* **2000,** *39* (17), 3738.
5. Ferrere, S., New Photosensitizers Based Upon $[Fe(L)_2(CN)_2]$ and $[Fe(L)_3]$ (L = Substituted 2,2'-Bipyridine): Yields for the Photosensitization of TiO_2 and Effects on the Band Selectivity. *Chem. Mater.* **2000,** *12*, 1083.
6. Ferrere, S.; Gregg, B. A., Photosensitization of TiO_2 by $[Fe^{II}$(2,2'-bipyridine-4,4'-dicarboxylic acid$)_2(CN)_2]$: Band Selective Electron Injection from Ultra-Short-Lived Excited States. *J. Am. Chem. Soc.* **1998,** *120* (4), 843.
7. Monat, J. E.; McCusker, J. K., Femtosecond Excited-State Dynamics of an Iron(II) Polypyridyl Solar Cell Sensitizer Model. *J. Am. Chem. Soc*. **2000,** *122* (17), 4092.
8. Yang, M.; Thompson, D. W.; Meyer, G. J., Charge-Transfer Studies of Iron Cyano Compounds Bound to Nanocrystalline TiO_2 Surfaces. *Inorg. Chem.* **2002,** *41* (5), 1254.
9. Létard, J. F.; Guionneau, P.; Goux-Capes, L., Towards Spin Crossover Applications. *Spin Crossover in Transition Metal Compounds III* **2004,** *1*, 1.
10. Gütlich, P.; Goodwin, H. A., Spin Crossover — an Overall Perspective. *Spin Crossover in Transition Metal Compounds I* **2004,** *1*, 1.
11. Ferrere, S., New Photosensitizers Based Upon $[Fe(L)_2(CN)_2]$ and $[Fe(L)_3]$ (L = substituted 2,2'-bipyridine): Yields for the Photosensitization of TiO_2 and Effects on the Band Selectivity. *Chem. Mater.* **2000,** *12*, 1083.
12. Ferrere, S., New Photosensitizers Based Upon $[Fe^{II}(L)_2(CN)_2]$ and $[Fe^{II}L_3]$, Where L Is Substituted 2,2′-bipyridine. *Inorg. Chim. Acta* **2002,** *329* (1), 79.
13. Ferrere, S.; Gregg, B. A., Photosensitization of TiO_2 by $[Fe^{II}$(2,2′-bipyridine-4,4′-dicarboxylic acid$)_2(CN)_2]$: Band Selective Electron Injection from Ultra-Short-Lived Excited States. *J. Am. Chem. Soc.* **1998,** *2*, 843.
14. Yang, M.; Thompson, D. W.; Meyer, G. J., Dual Pathways for TiO_2 Sensitization by $Na_2[Fe(bpy)(CN)_4]$. *Inorg. Chem.* **2000,** *39*, 3738.
15. Yang, M.; Thompson, D. W.; Meyer, G. J., Charge-Transfer Studies of Iron Cyano Compounds Bound to Nanocrystalline Tio2 Surfaces. *Inorg. Chem.* **2002,** *41*, 1254.
16. Monat, J. E.; McCusker, J. K., Femtosecond Excited-State Dynamics of an Iron(II) Polypyridyl Solar Cell Sensitizer Model. *J. Am. Chem. Soc*. **2000,** *122*, 4092.
17. Juban, E. A.; Smeigh, A. L.; Monat, J. E.; McCusker, J. K., Ultrafast Dynamics of Ligand-Field Excited States. *Coord. Chem. Rev.* **2006,** *250* (13-14), 1783.
18. Smeigh, A. L.; Creelman, M.; Mathies, R. a.; McCusker, J. K., Femtosecond Time-Resolved Optical and Raman Spectroscopy of Photoinduced Spin Crossover: Temporal Resolution of Low-to-High Spin Optical Switching. *J. Am. Chem. Soc.* **2008,** *130*, 14105.
19. Lawson Daku, L. M.; Vargas, A.; Hauser, A.; Fouqueau, A.; Casida, M. E., Assessment of Density Functionals for the High-Spin/Low-Spin Energy Difference in the Low-Spin Iron(II) tris (2,2 -bipyridine) Complex. *ChemPhysChem* **2005,** *6*, 1393.
20. Paulsen, H.; Duelund, L.; Winkler, H.; Toftlund, H.; Trautwein, A. X., Free Energy of Spin-Crossover Complexes Calculated with Density Functional Methods. *Inorg. Chem.* **2001,** *40*, 2201.

21. Shiota, Y.; Sato, D.; Juha sz, G.; Yoshizawa, K., Theoretical Study of Thermal Spin Transition between the Singlet State and the Quintet State in the $[Fe(2\text{-picolylamine})_3]^{2+}$ Spin Crossover System. *J. Phys. Chem. A* **2010,** *114*, 5862.
22. Zein, S.; Matouzenko, G. S.; Borshch, S. A., Quantum Chemical Study of Three Polymorphs of the Mononuclear Spin-Transition Complex $[Fe(dppa)(NCS)_2]$. *J. Phys. Chem. A* **2005,** *109*, 8568.
23. Paulsen, H.; Trautwein, A., Density Functional Theory Calculations for Spin Crossover Complexes. *Spin Crossover in Transition Metal Compounds III* **2004**, 355.
24. Paulsen, H.; Duelund, L.; Zimmermann, A.; Averseng, F. d. r.; Gerdan, M.; Winkler, H.; Toftlund, H.; Trautwein, A. X., Substituent Effects on the Spin-Transition Temperature in Complexes with Tris(Pyrazolyl) Ligands. *Monatshefte fur Chemie* **2003,** *134*, 295.
25. Reiher, M., Theoretical Study of the Fe(Phen)2(Ncs)2 Spin-Crossover Complex with Reparametrized Density Functionals. *Inorg. Chem.* **2002,** *41*, 6928.
26. Reiher, M.; Salomon, O.; Artur Hess, B., Reparameterization of Hybrid Functionals Based on Energy Differences of States of Different Multiplicity. *Theor. Chem. Acc.* **2001,** *107*, 48.
27. Salomon, O.; Reiher, M.; Hess, B. A., Assertion and Validation of the Performance of the B3LYP* Functional for the First Transition Metal Row and the G2 Test Set. *J. of Chem. Phys.* **2002,** *117*, 4729.
28. Swart, M., Accurate Spin-State Energies for Iron Complexes. *J. Chem. Theory Comput.* **2008,** *4*, 2057.
29. de Graaf, C.; Sousa, C., Study of the Light-Induced Spin Crossover Process of the $[Fe(II)(bpy)_3]^{2+}$ Complex. *Chemistry (Weinheim an der Bergstrasse, Germany)* **2010,** *16*, 4550.
30. Bolvin, H., D → D Spectrum and High-Spin/Low-Spin Competition in d^6 Octahedral Coordination Compounds: Ab Initio Study of Potential Energy Curves. *J. Phys. Chem. A* **1998,** *102* (38), 7525.
31. Becke, A. D., Density-Functional Thermochemistry. Iii. The Role of Exact Exchange. *J. Chem. Phys.* **1993,** *98*, 5648.
32. Dolg, M.; Wedig, U.; Stoll, H.; Preuss, H., Energy-Adjusted Ab Initio Pseudopotentials for the First Row Transition Elements. *J. Chem. Phys.* **1987,** *86*, 866.
33. Krishnan, R.; Binkley, J. S.; Seeger, R.; Pople, J. A., Self-Consistent Molecular-Orbital Methods .20. Basis Set for Correlated Wave-Functions. *J. Chem. Phys.* **1980,** *72* (1), 650.
34. Clark, T.; Chandrasekhar, J.; Spitznagel, G. W.; Schleyer, P. V. R., Efficient Diffuse Function-Augmented Basis Sets for Anion Calculations. III. The 3-21+G Basis Set for First-Row Elements, Li–F. *J. Comput. Chem.* **1983,** *4* (3), 294.
35. Hohenberg, P.; Kohn, W., Inhomogeneous Electron Gas. *Phys. Rev. B* **1964,** *136*, 864.
36. Becke, A. D., Density-Functional Exchange-Energy Approximation with Correct Asymptotic Behavior. *Phys. Rev. A* **1988,** *38* (6), 3098.
37. Perdew, J. P.; Chevary, J. A.; Vosko, S. H.; Jackson, K. A.; Pederson, M. R.; Singh, D. J.; Fiolhais, C., Atoms, Molecules, Solids, and Surfaces - Applications of the Generalized Gradient Approximation for Exchange and Correlation. *Phys. Rev. B* **1992,** *46* (11), 6671.
38. Bauernschmitt, R.; Ahlrichs, R., Stability Analysis for Solutions of the Closed Shell Kohn-Sham Equation. *J. Chem. Phys.* **1996,** *104* (22), 9047.
39. Seeger, R.; Pople, J. A., Self-Consistent Molecular-Orbital Methods. 18. Constraints and Stability in Hartree-Fock Theory. *J. Chem. Phys.* **1977,** *66* (7), 3045.
40. Scalmani, G.; Frisch, M. J., Continuous Surface Charge Polarizable Continuum Models of Solvation. I. General Formalism. *J. Chem. Phys.* **2010,** *132* (11), 114110.
41. Frisch, M. J. T., G. W.; Schlegel, H. B.; Scuseria, G. E.; Robb, M. A.; Cheeseman, J. R.; Scalmani, G.; Barone, V.; Mennucci, B.; Petersson, G. A.; Nakatsuji, H.; Caricato, M.; Li, X.; Hratchian, H. P.; Izmaylov, A. F.; Bloino, J.; Zheng, G.; Sonnenb, D. J., Gaussian 09, Revision A.02. Gaussian, Inc.: Wallingford CT, 2009.
42. Carter, E. A.; Goddard, W. A., Relationships between Bond Energies in Coordinatively Unsaturated and Coordinatively Saturated Transition-Metal Complexes: A Quantitative Guide for Single, Double, and Triple Bonds. *J. Phys. Chem.* **1988,** *92* (20), 5679.
43. Yanagisawa, S.; Tsuneda, T.; Hirao, K., An Investigation of Density Functionals: The First-Row Transition Metal Dimer Calculations. *J. Chem. Phys.* **2000,** *112* (2), 545.

44. Shaik, S.; Hirao, H.; Kumar, D., Reactivity of High-Valent Iron–Oxo Species in Enzymes and Synthetic Reagents: A Tale of Many States. *Acc. Chem. Res.* **2007,** *40* (7), 532.
45. Stephens, P.; Devlin, F., Ab Initio Calculation of Vibrational Absorption and Circular Dichroism Spectra Using Density Functional Force Fields. *J. Phys. Chem.* **1994,** *98*, 11623.
46. Stratmann, R. E.; Scuseria, G. E.; Frisch, M. J., An Efficient Implementation of Time-Dependent Density-Functional Theory for the Calculation of Excitation Energies of Large Molecules. *J. Chem. Phys.* **1998,** *109* (19), 8218.
47. Casida, M. E.; Jamorski, C.; Casida, K. C.; Salahub, D. R., Molecular Excitation Energies to High-Lying Bound States from Time-Dependent Density-Functional Response Theory: Characterization and Correction of the Time-Dependent Local Density Approximation Ionization Threshold. *J. Chem. Phys.* **1998,** *108* (11), 4439.
48. Bauernschmitt, R.; Ahlrichs, R., Treatment of Electronic Excitations within the Adiabatic Approximation of Time Dependent Density Functional Theory. *Chem. Phys. Lett.* **1996,** *256* (4-5), 454.
49. Scalmani, G.; Frisch, M. J., Continuous Surface Charge Polarizable Continuum Models of Solvation. I. General Formalism. *J. Chem. Phys.* **2010,** *132* (11).
50. Kresse, G.; Furthmüller, J., Efficiency of Ab-Initio Total Energy Calculations for Metals and Semiconductors Using a Plane-Wave Basis Set. *Comput. Mat. Sci.* **1996,** *6*, 15.
51. Kresse, G.; Furthmüller, J., Efficient Iterative Schemes for Ab Initio Total-Energy Calculations Using a Plane-Wave Basis Set. *Phys. Rev. B* **1996,** *54*, 11169.
52. Kresse, G.; Hafner, J., Ab Initio Molecular Dynamics for Liquid Metals. *Physical Review B* **1993,** *47*, 558.
53. Kresse, G.; Hafner, J., Ab Initio Molecular-Dynamics Simulation of the Liquid-Metal-Amorphous-Semiconductor Transition in Germanium. *Phys. Rev. B* **1994,** *49*, 14251.
54. Perdew, J.; Burke, K.; Ernzerhof, M., Generalized Gradient Approximation Made Simple. *Phys. Rev. Lett.* **1996,** *77*, 3865.
55. Perdew, J.; Burke, K.; Ernzerhof, M., Errata: Generalized Gradient Approximation Made Simple. Generalized Gradient Approximation Made Simple [Phys. Rev. Lett. 77, 3865 (1996)]. *Phys. Rev. Lett.* **1997,** *78*, 1396.
56. Blöchl, P. E., Projector Augmented-Wave Method. *Phys. Rev. B* **1994,** *50*, 17953.
57. Kresse, G.; Joubert, D., From Ultrasoft Pseudopotentials to the Projector Augmented-Wave Method. *Phys. Rev. B* **1999,** *59*, 1758.
58. Kabsch, W., A Discussion of the Solution for the Best Rotation to Relate Two Sets of Vectors. *Acta Crystallogr., Sect. A: Found. Crystallogr.* **1978,** *34*, 827.
59. Rego, L. G. C.; Batista, V. S., Quantum Dynamics Simulations of Interfacial Electron Transfer in Sensitized Tio2 Semiconductors. *J. Am. Chem. Soc.* **2003,** *125*, 7989.
60. Jakubikova, E.; Snoeberger Iii, R. C.; Batista, V. S.; Martin, R. L.; Batista, E. R., Interfacial Electron Transfer in TiO_2 Surfaces Sensitized with Ru(II)−Polypyridine Complexes. *J. Phys. Chem. A* **2009,** *113* (45), 12532.
61. Nieuwenhuyzen, M.; Bertram, B.; Gallagher, J.; Vos, J., Dipotassium (2,2'-bipyridyl-N,N')-tetracyanoferrate(II) 2.5-Hydrate, $K_2[Fe(bpy)(CN)_4].2.5H_20$. *Acta Crystallogr., Sect. C: Cryst. Struct. Commun.* **1998,** *54*, 603.
62. Ma, B. Q.; Sun, H. L.; Gao, S., Vertex-Sharing Water Tape Consisting of Cyclic Hexamers. *Eur. J. Inorg. Chem.* **2005,** (19), 3902.
63. Persson, P.; Lunell, S., Binding of Bi-Isonicotinic Acid to Anatase TiO_2 (101). *Sol. Energy Mater. Sol. Cells* **2000,** *63* (2), 139.
64. De Angelis, F.; Tilocca, A.; Selloni, A., Time-Dependent DFT Study of $[Fe(CN)_6]^{4-}$ Sensitization of TiO_2 Nanoparticles. *J. Am. Chem. Soc.* **2004,** *126*, 15024.
65. Schilt, A. A., Mixed Ligand Complexes of Iron (II) and (III) with Cyanide and Aromatic Di-Imines. *J. Am. Chem. Soc.* **1960,** *82*, 3000.
66. Gütlich, P.; Garcia, Y.; Goodwin, H. A., Spin Crossover Phenomena in Fe(II) Complexes. *Chem. Soc. Rev.* **2000,** *29*, 419.

67. Konno, M. M.-K., M., Temperatue- or Pressure-Induced Structure Changes of a Spin Crossover Fe(II) Complex; [Fe(bpy)$_2$(NCS)$_2$]. *Bull. Chem. Soc. Jpn.* **1991,** *64*, 339.
68. Bruno, I. J.; Cole, J. C.; Edgington, P. R.; Kessler, M.; Macrae, C. F.; McCabe, P.; Pearson, J.; Taylor, R., New Software for Searching the Cambridge Structural Database and Visualizing Crystal Structures. *Acta Crystallogr., Sect. B: Struct. Sci.* **2002,** *58*, 389.
69. Medlycott, E. A.; Hanan, G. S.; Abedin, T. S. M.; Thompson, L. K., The Effect of Steric Hindrance on the Fe(II) Complexes of Triazine-Containing Ligands. *Polyhedron* **2008,** *27*, 493.
70. Chang, H. R.; McCusker, J. K.; Toftlund, H.; Wilson, S. R.; Trautwein, A. X.; Winkler, H.; Hendrickson, D. N., (Tetrakis(2-Pyridylmethyl)Ethylenediamine)Iron(Ii) Perchlorate , the First Rapidly Interconverting Ferrous Spin-Crossover Complex. *J. Am. Chem. Soc.* **1990,** *112*, 6814.
71. Chambers, J.; Eaves, B.; Parker, D.; Claxton, R.; Ray, P. S.; Slattery, S. J., Inductive Influence of 4′-Terpyridyl Substituents on Redox and Spin State Properties of Iron(II) and Cobalt(II) Bis-Terpyridyl Complexes. *Inorg. Chim. Acta* **2006,** *359* (8), 2400.
72. Khalil, M.; Marcus, M. A.; Smeigh, A. L.; McCusker, J. K.; Chong, H. H. W.; Schoenlein, R. W., Picosecond X-Ray Absorption Spectroscopy of a Photoinduced Iron (II) Spin Crossover Reaction in Solution. *J. Phys. Chem. A* **2006,** *110*, 38.
73. Figgis, B. N.; Hitchman, M. A., *Ligand Field Theory and Its Applications*. Wiley-VCH: New York, 2000; p 354.
74. Levanon, H.; Stein, G.; Luz, Z., The Electron Spin Resonance Spectrum of (Fef6)3- in Aqueous Solutions. *J. Am. Chem. Soc* **1968,** *90*, 5292.
75. Podesta, T. J.; Orpen, A. G., Tris(Pyridinium)Triazine in Crystal Synthesis of 3-Fold Symmetric Structures. *Cryst. Growth Des.* **2005,** *5* (2), 681.
76. Sim, P. G.; Sinn, E., Synthesis and Crystal Structure of tris[1-(2-azolyl)-2-azabuten-4-yl] amineiron (III), [Fe((pyrol)$_3$tren)]. *Inorg. Chem.* **1978,** *17*, 1288.
77. Guionneau, P.; Marchivie, M.; Garcia, Y.; Howard, J.; Chasseau, D., Spin Crossover in [Mn^{III}(pyrol)$_3$tren] Probed by High-Pressure and Low-Temperature X-Ray Diffraction. *Phys. Rev. B* **2005,** *72*, 1.
78. Sieber, R.; Decurtins, S.; Stoeckli-Evans, H.; Wilson, C.; Yufit, D.; Howard, J. A. K.; Capelli, S. C.; Hauser, A., A Thermal Spin Transition in [Co(bpy)$_3$][LiCr(ox)$_3$] (ox=$C_2O_4^{2-}$; bpy=2,2'-bipyridine). *Chem. Eur. J* **2000,** *6*, 361.
79. Figgis, B., Crystal Structure of bis(2,2':6',2"-terpyridyl)Cobalt(II) perchlorate c. 1.3 hydrate. *Aust. J. Chem.* **1983,** *36*, 1537.
80. Allen, G.; Warren, K., The Electronic Spectra of the Hexafluoro Complexes of the First Transition Series. In *Structure and Bonding*, Springer Berlin / Heidelberg: **1971**; Vol. 9, pp 49.
81. Romero, R.; Morales, A.; Rodríguez, J.; Bertrán, J., Crystal Structure of Potassium Tetramethylammonium Hexacyanocobaltate(III) Trihydrate**:** $K_3(Me_4N)_3[Co(CN)_6]_2\cdot 3H_2O$**.** *Transition Met. Chem.* **1992**, *17* (6), 573.
82. Wang, X.-Y.; Justice, R.; Sevov, S. C., Hydrogen-Bonded Metal-Complex Sulfonate (Mcs) Inclusion Compounds: Effect of the Guest Molecule on the Host Framework. *Inorg. Chem.* **2007,** *46* (11), 4626.

8. Tables

Table 1. Experimental and calculated spin multiplicity of pseudo-octahedral first row transition metal complexes investigated in this work. * denotes thermal spin crossover complexes.

Complex	Ground State (Experimental)	Ground State (Δ*E*, B3LYP/SDD, 6-311+G*)	Ground State at 273.15 K (Δ*G*, B3LYP/SDD, 6-311+G*)
$[Fe(bpy)_2(CN)_2]^0$	Singlet[65]	Singlet	Quintet
$[Fe(bpy)(CN)_4]^{2-}$	Singlet[65]	Singlet	Singlet
$[Fe(CN)_6]^{4-}$	Singlet[66]	Singlet	Singlet
$[Fe(bpy)_2(NCS)_2]^0$	Singlet*[67]	Quintet	Quintet
$[Fe(bpy)_2Cl_2]^0$	Quintet[68]	Quintet	Quintet
$[Fe(bpy)_3]^{2+}$	Singlet[66]	Singlet	Quintet
$[Fe(phen)_3]^{2+}$	Singlet[66]	Quintet	Quintet
$[Fe(Lt)_2]^{2+}$	Singlet[69]	Quintet	Quintet
[Fe(Me-Lt)2]$^{2+}$	Quintet[69]	Quintet	Quintet
[Fe(tpen)]$^{2+}$	Singlet*[70]	Quintet	Quintet
$[Fe(terpy)_2]^{2+}$	Singlet[71]	Quintet	Quintet
[Fe(tren(py)3)]$^{2+}$	Singlet[72]	Quintet	Quintet
$[Fe(tren(6\text{-}Me\text{-}py)_3)]^{2+}$	Quintet[72]	Quintet	Quintet
$[Fe(H_2O)_6]^{2+}$	Quintet[66]	Quintet	Quintet
$[Fe(NH_3)_6]^{2+}$	Quintet[73]	Quintet	Quintet
$[Fe(NH_3)_6]^{3+}$	Sextet[73]	Doublet	Sextet
$[FeF_6]^{3-}$	Sextet[74]	Sextet	Sextet
$[FeCl_6]^{3-}$	Sextet[75]	Sextet	Sextet
$[Fe(pyrol)_3tren]^0$	Doublet[76]	Doublet	Sextet
$[Mn(pyrol)_3tren]^0$	Quintet[77]	Quintet	Quintet
$[Co(bpy)_3]^{2+}$	Quartet[78]	Quartet	Quartet
$[Co(terpy)_2]^{2+}$	Doublet*[79]	Quartet	Quartet
$[CoF_6]^{3-}$	Quintet[80]	Quintet	Quintet
$[Co(CN)_6]^{3-}$	Singlet[81]	Singlet	Singlet
$[Co(NH_3)_6]^{3+}$	Singlet[82]	Singlet	Singlet

Table 2. Table of average change in metal – ligand bond lengths ΔR(metal-ligand) in Ångstroms for low spin to high spin transition versus slope of the scan over the exact exchange for various pseudo-octahedral complexes. * $[Os(bpy)_3]^{2+}$ quintet changes electronic states over the exact exchange admixture investigated.

Complex	**ΔR (metal-ligand) [Å]**	Slope of Scan $\frac{d(\Delta E)}{dc_1}$	Slope of Scan $\frac{d(\Delta H)}{dc_1}$	Slope of Scan $\frac{d(\Delta G)}{dc_1}$
$[Fe(CN)_6]^{4-}$	0.3336	-214.17	-212.51	-208.92
$[Fe(bpy)(CN)_4]^{2-}$	0.2726	-185.56	-184.48	-181.69
$[Fe(bpy)_2(CN)_2]^{0}$	0.2337	-161.42	-160.73	160.02
$[Co(CN)_6]^{3-}$	0.2295	-145.62	-143.93	-137.59
$[Fe(Lt)_2]^{2+}$	0.2266	-160.18	-158.10	-161.41
$[Fe(tren(py)_3)]^{2+}$	0.2265	-147.79	-146.01	-141.98
$[Fe(terpy)_2]^{2+}$	0.2149	-156.18	-154.86	-152.45
$[Fe(tren(6\text{-}Me\text{-}py)_3)]^{2+}$	0.2125	-142.97	-141.98	-142.88
$[Fe(tpen)]^{2+}$	0.2044	-125.25	-124.52	-117.40
$[Fe(bpy)_3]^{2+}$	0.2013	-143.56	-143.20	-141.62
$[Fe(bpy)_2(NCS)_2]^{0}$	0.2003	-125.76	-124.30	-124.48
$[Fe(phen)_3]^{2+}$	0.1994	-139.34	-139.67	-138.29
$[Fe(Me\text{-}Lt)_2]^{2+}$	0.1991	-142.16	-149.73	-156.79
$[Fe(NH_3)_6]^{2+}$	0.1827	-91.95	-92.05	-90.70
$[Fe(bpy)_2Cl_2]^{0}$	0.1755	-126.90	-127.05	-127.54
$[Fe(pyrol)_3tren]^{0}$	0.1655	-97.80	-96.84	-92.48
$[Co(NH_3)_6]^{3+}$	0.1561	-88.39	-90.37	-93.56
$[Fe(NH_3)_6]^{3+}$	0.1498	-89.33	-92.26	-93.07
$[Co(bpy)_3]^{2+}$	0.1290	-89.33	-89.55	-87.59
$[Fe(H_2O)_6]^{2+}$	0.1230	-62.12	-62.24	-63.08
$[Co(terpy)_2]^{2+}$	0.1136	-93.29	-90.49	-97.06
$[Mn(pyrol)_3tren]^{0}$	0.1095	-58.44	-58.88	-57.12
$[FeCl_6]^{3-}$	0.0908	-54.97	-54.51	-49.97
$[CoF_6]^{3-}$	0.0638	-45.42	-38.17	-30.97
$[FeF_6]^{3-}$	0.0610	-48.25	-47.47	-42.93
$[Ru(bpy)_3]^{2+}$	0.2760	-109.44	-108.74	-112.39
$[Os(bpy)_3]^{2+}$	0.1372	-16.74*	-9.21*	-17.89*

Table 3. Table of metal ligand bond lengths for the complexes investigated, coordination site labeling corresponds with Figure 6.

Iron-Ligand Bond	**$[Fe(bpy)(CN)_4]^{2-}$ 1**	**$[Fe(bpy\text{-}dca)(CN)_4]^{2-}$ 2**	**$[Fe(bpy\text{-}dca)_2(CN)_2]$ 3**
	Length (Å)	Length (Å)	Length (Å)
Fe-L1 (CN^-)	1.959	1.955	1.942
Fe-L2 (CN^-)	1.988	1.977	1.942
Fe-L3 (CN^-, bpy)	1.959	1.955	2.020
Fe-L4 (CN^-, bpy)	1.989	1.977	1.996
Fe-L5 (bpy)	1.992	1.959	2.020
Fe-L6 (bpy)	1.992	1.963	1.998

9. Figure Captions

Figure 1. Fe(II) complexes investigated in this work

Figure 2. Heteropyridine ligands considered in this study.

Figure 3. Dependence of the energy difference, $\Delta E_{HS/LS} = E_{high-spin} - E_{low-spin}$ (kcal/mol), on the exact exchange admixture (c_1) in the B3LYP functional for iron pseudo-octahedral complexes with various ligands: $[Fe(CN)_6]^{4-}$ (1), $[Fe(bpy)_2(CN)_2]^0$ (2), $[Fe(bpy)_3]^{2+}$ (3), $[Fe(NH_3)_6]^{3+}$ (4), $[FeCl_6]^{3-}$ (5). $\Delta E_{HS/LS} > 0$ corresponds to the low-spin ground state (singlet or doublet), $\Delta E_{HS/LS} < 0$ corresponds to the high-spin ground state (quintet or sextet).

Figure 4. Plot of average change in metal to ligand bond lengths in transition from low-spin to high-spin states versus slope of the scan over exact exchange for data shown in Table 2 along with a plot of the linear regression, R^2=0.93.

Figure 5. Dependence of the energy difference, $\Delta E_{HS/LS} = E_{high-spin} - E_{low-spin}$ $\Delta E_{HS/LS} = E_{high-spin} - E_{low-spin}$ (kcal/mol), on the exact exchange admixture (c_1) in the B3LYP functional for several pseudo-octahedral iron(II)-polypyridine complexes: $[Fe(bpy)_2(CN)_2]^0$ (**1**), $[Fe(bpy)_3]^{2+}$ (**2**), $[Fe(tren(py)_3)]^{2+}$ (**3**), $[Fe(bpy)_2(NCS)_2]^0$ (**4**), $[Fe(tren(6\text{-}Me\text{-}py)_3)]^{2+}$ (**5**), and $[Fe(bpy)_2Cl_2]^0$ (**6**). $\Delta E_{HS/LS} > 0$ $\Delta E_{HS/LS} > 0$ corresponds to the singlet ground state, $\Delta E_{HS/LS} < 0$ $\Delta E_{HS/LS} < 0$ corresponds to the quintet ground state. A linear regression is plotted for each complex based on the constant slope formula $\Delta E_{HS/LS} = I - 140.2c_1$.

Figure 6. Optimized structures of dyes **1**, **2**, and **3** with each coordination site labeled (L1-L6).

Figure 7. Simulated absorption spectra for (from top to bottom) dyes **1, 2**, and **3** with Lorentzian broadening of HWMH = 0.12 eV with important excitations ($f_{osc} > 0.01$) in the visible region labeled, calculated with B3LYP TD-DFT in PCM (acetonitrile).

Figure 8. Relevant particle states for the major excitations ($f_{osc} > 0.01$) from the calculated spectra shown in Figure 7. Kohn-Sham orbitals are classified by the absorption band (columns) and by similarity in nodal structure (rows).

Figure 9. Optimized structures of anatase (101) with pyridine-4-carboxylic acid binding via a monodentate (a) and bidentate (b) binding mode, and hydrogen cyanide (c).

Figure 10. Final slab models of dye-nanoparticle assemblies consisting of $[Fe(bpy\text{-}dca)_2(CN)_2]$ attached to anatase (101) via a monodentate carboxylic acid binding mode in the following nonequivalent orientations: bpy parallel (left) and bpy perpendicular (right).

Figure 11. Structure of **1**-TiO_2 assembly employing CN^- as the anchoring group.

Figure 12. Density of states for **1**-TiO_2 anatase (101) slab model (left) and enlarged conduction band (right) show the following: total density of states (blue line), projected density of states on the dye (black line), and the energy levels of the dye in vacuum using extended Hückel (black level set lines). Gaussian line-shape (HWHM = 0.05 eV) used for convolution.

Figure 13. Discrete energy levels of the dyes (left) in vacuum, using extended Hückel level of theory, showing the evolution of the similar molecular orbitals, going from the smallest to the largest dye. The DOS/pDOS for the $[Fe(bpy\text{-}dca)_2(CN)_2]/TiO_2$ nanoparticle system is shown for reference (right).

Figure 14. Characteristic interfacial electron transfer times for relevant particle states of $[Fe(bpy)(CN)_4]^{2-}$ attached to anatase (101) slab in both the "bpy parallel" and "bpy perpendicular" orientations via monodentate cyanide anchoring groups with varying nitrogen titanium distances (2.33, 2.22, and 2.12 Å), determined by either exponential or biexponential fitting.

Figure 15. Characteristic interfacial electron transfer times for relevant particle states of $[Fe(bpy\text{-}dca)(CN)_4]^{2-}$ attached to anatase (101) slab by monodentate carboxylic acid, bidentate carboxylic acid, and cyanide anchoring groups (in both the "bpy parallel" and "bpy perpendicular" orientations), determined by either exponential or biexponential fitting.

Figure 16. Characteristic interfacial electron transfer times for relevant particle states of $[Fe(bpy\text{-}dca)_2(CN)_2]$ attached to anatase (101) slab by monodentate carboxylic acid (in both the "bpy parallel" and "bpy perpendicular" orientations), bidentate carboxylic acid (in both the "bpy parallel" and "bpy perpendicular" orientations), and cyanide anchoring groups, determined by either exponential or biexponential fitting.

10. Figures

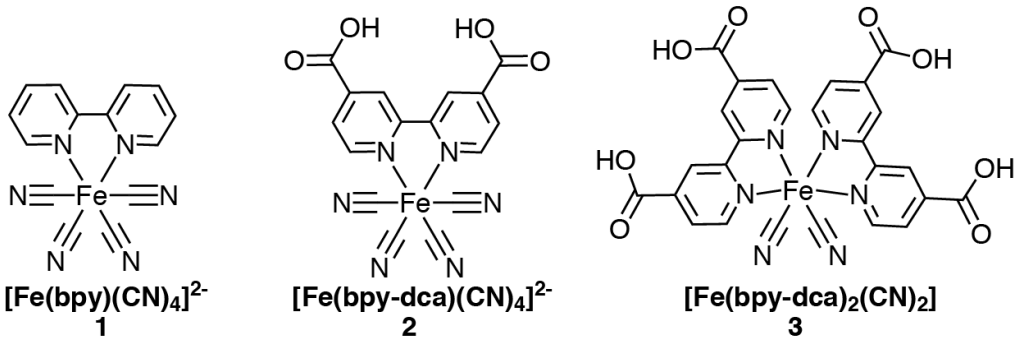

Figure 1. Fe(II) complexes investigated in this work

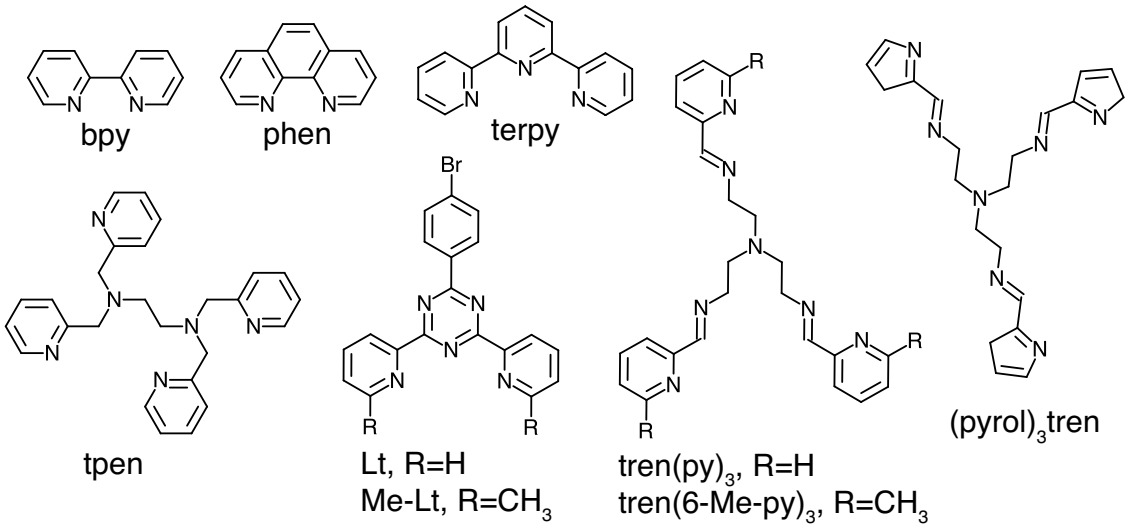

Figure 2. Heteropyridine ligands considered in this study.

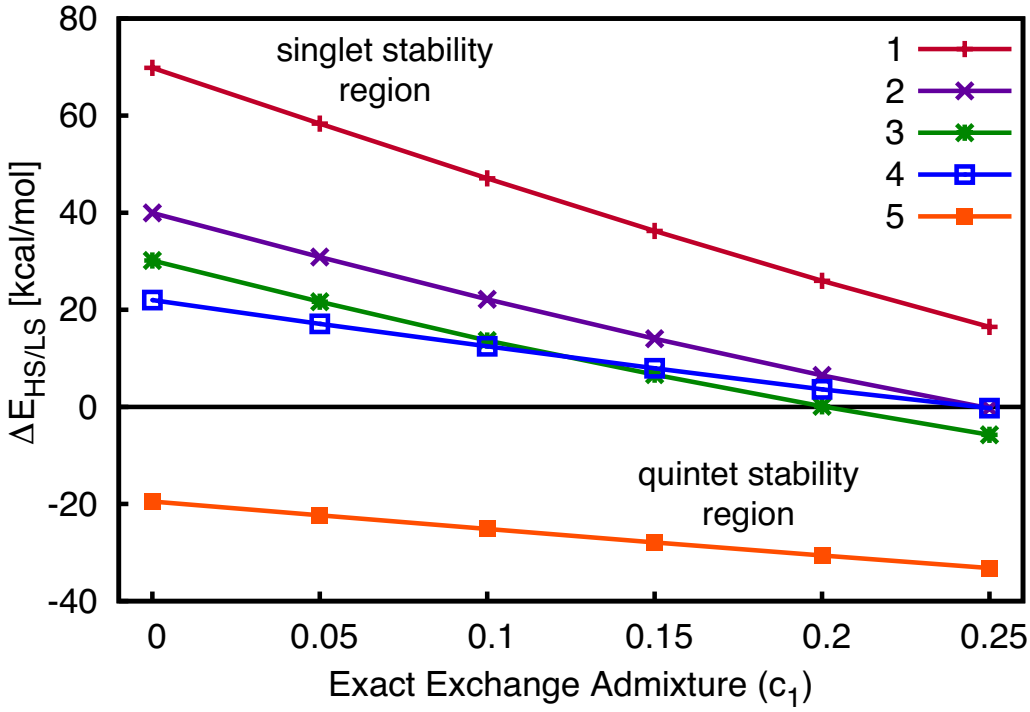

Figure 3. Dependence of the energy difference, $\Delta E_{HS/LS} = E_{high-spin} - E_{low-spin}$ (kcal/mol), on the exact exchange admixture (c_1) in the B3LYP functional for iron pseudo-octahedral complexes with various ligands: $[Fe(CN)_6]^{4-}$ (1), $[Fe(bpy)_2(CN)_2]^0$ (2), $[Fe(bpy)_3]^{2+}$ (3), $[Fe(NH_3)_6]^{3+}$ (4), $[FeCl_6]^{3-}$ (5). $\Delta E_{HS/LS} > 0$ corresponds to the low-spin ground state (singlet or doublet), $\Delta E_{HS/LS} < 0$ corresponds to the high-spin ground state (quintet or sextet).

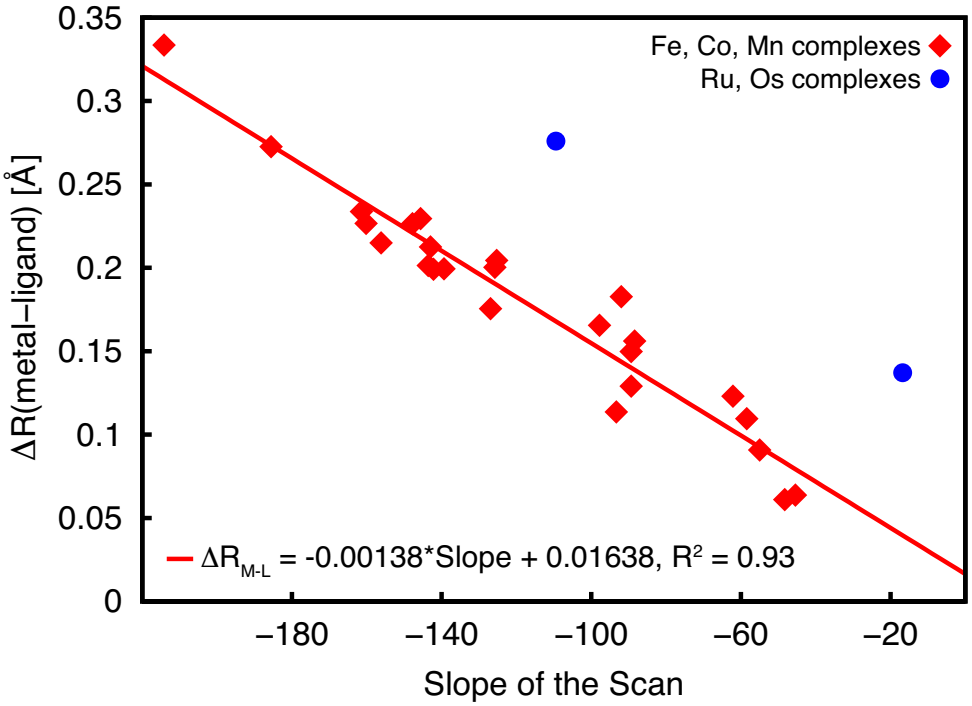

Figure 4. Plot of average change in metal to ligand bond lengths in transition from low-spin to high-spin states versus slope of the scan over exact exchange for data shown in Table 2 along with a plot of the linear regression, R^2=0.93.

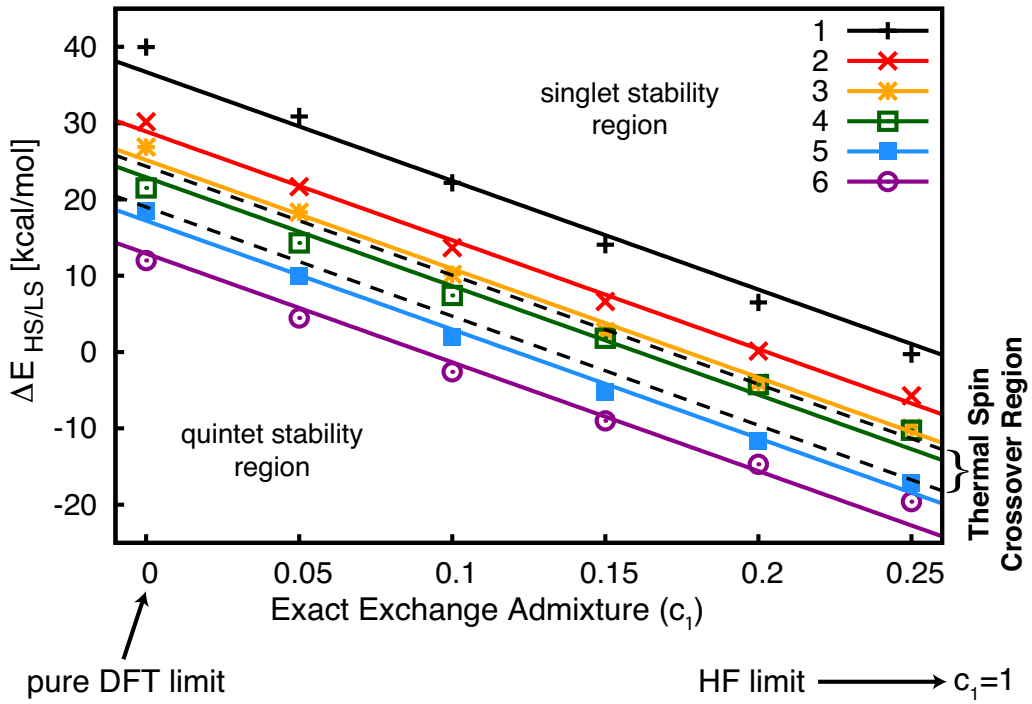

Figure 5. Dependence of the energy difference, $\Delta E_{HS/LS} = E_{high-spin} - E_{low-spin}$ $\Delta E_{HS/LS} = E_{high-spin} - E_{low-spin}$ (kcal/mol), on the exact exchange admixture (c_1) in the B3LYP functional for several pseudo-octahedral iron(II)-polypyridine complexes: $[Fe(bpy)_2(CN)_2]^0$ (**1**), $[Fe(bpy)_3]^{2+}$ (**2**), $[Fe(tren(py)_3)]^{2+}$ (**3**), $[Fe(bpy)_2(NCS)_2]^0$ (**4**), $[Fe(tren(6\text{-}Me\text{-}py)_3)]^{2+}$ (**5**), and $[Fe(bpy)_2Cl_2]^0$ (**6**). $\Delta E_{HS/LS} > 0$ $\Delta E_{HS/LS} > 0$ corresponds to the singlet ground state, $\Delta E_{HS/LS} < 0$ $\Delta E_{HS/LS} < 0$ corresponds to the quintet ground state. A linear regression is plotted for each complex based on the constant slope formula $\Delta E_{HS/LS} = I - 140.2c_1$ $\Delta E_{HS/LS} = I - 140.2c_1$

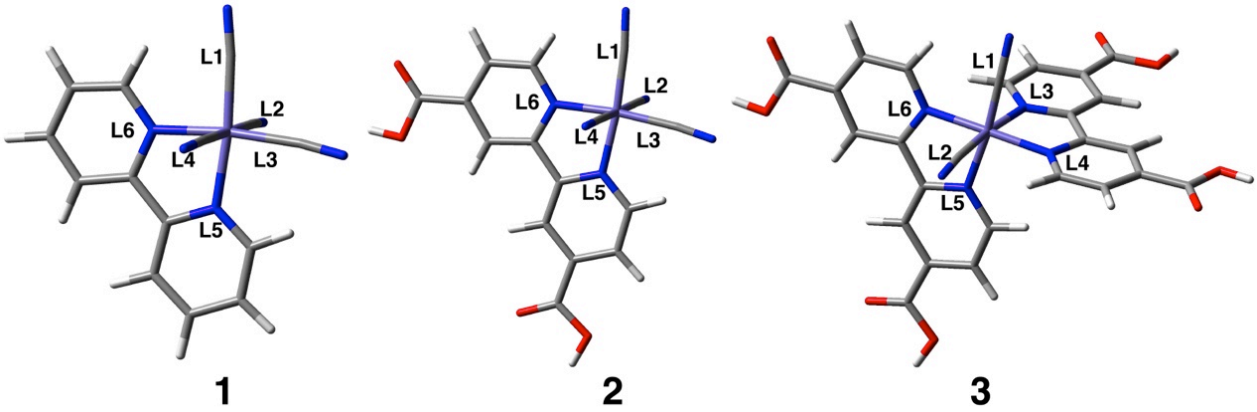

Figure 6. Optimized structures of dyes **1**, **2**, and **3** with each coordination site labeled (L1-L6).

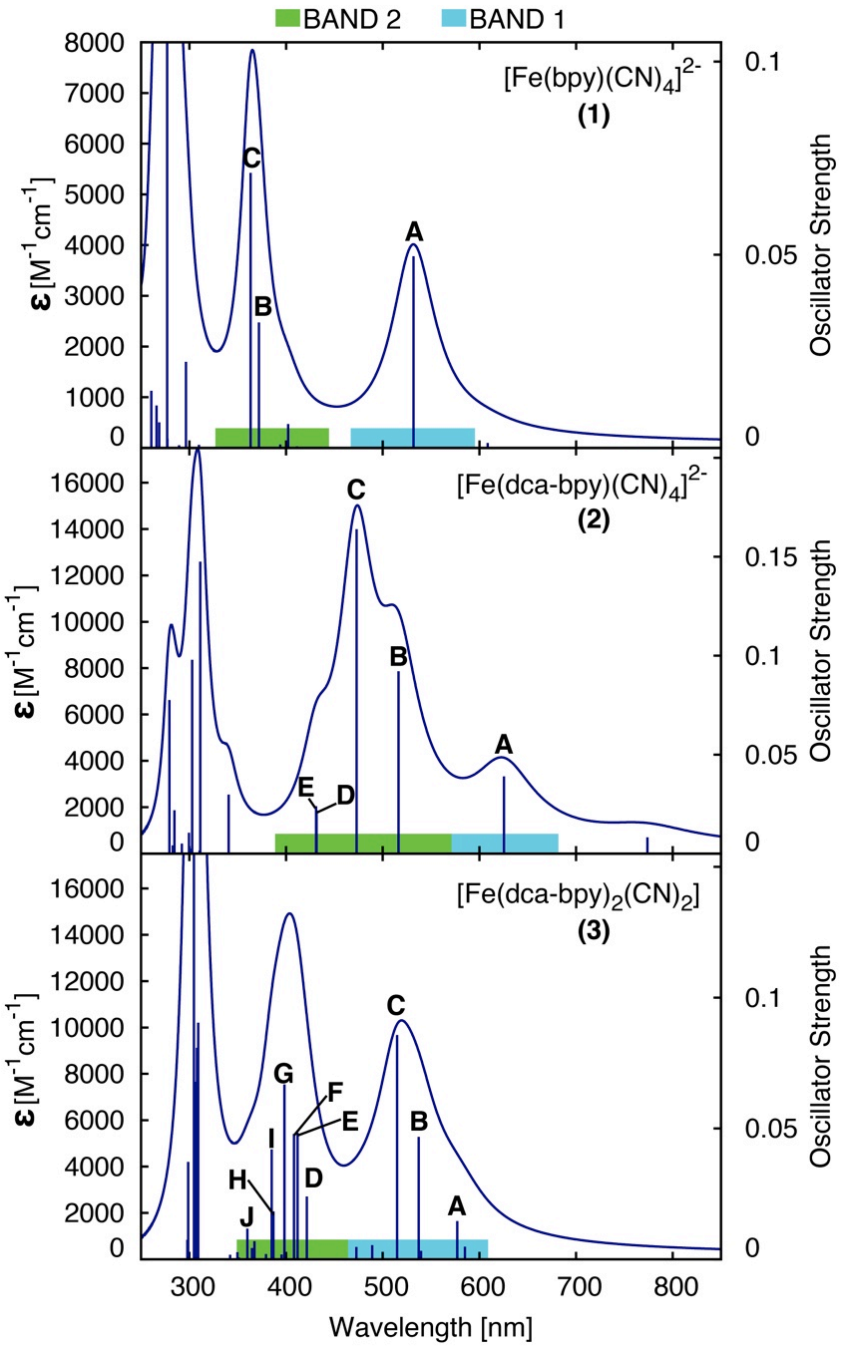

Figure 7. Simulated absorption spectra for (from top to bottom) dyes **1, 2**, and **3** with Lorentzian broadening of HWMH = 0.12 eV with important excitations (f_{osc} > 0.01) in the visible region labeled, calculated with B3LYP TD-DFT in PCM (acetonitrile).

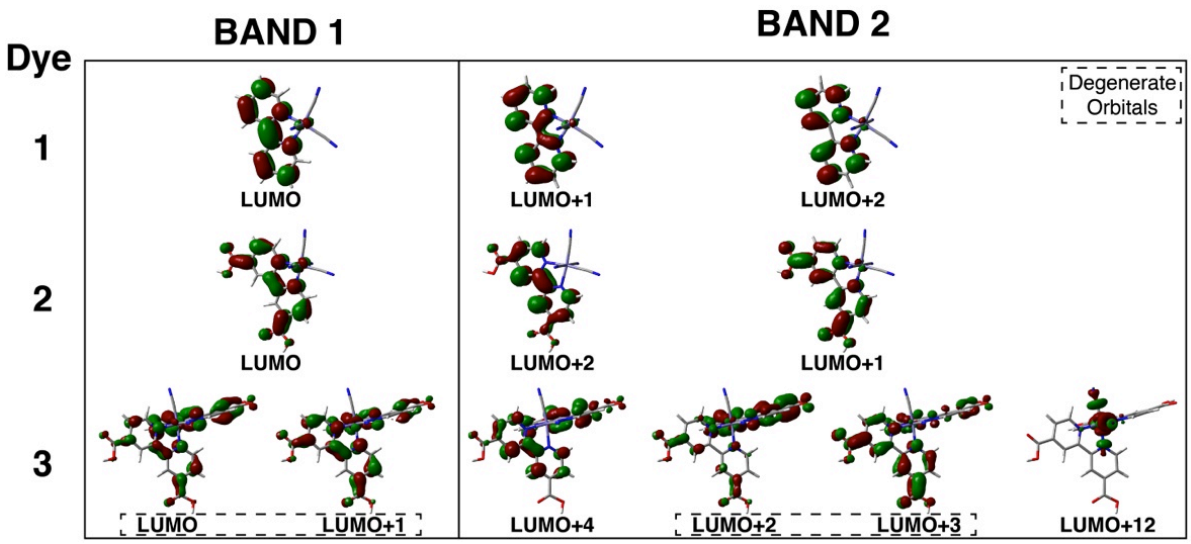

Figure 8. Relevant particle states for the major excitations ($f_{osc} > 0.01$) from the calculated spectra shown in Figure 7. Kohn-Sham orbitals are classified by the absorption band (columns) and by similarity in nodal structure (rows).

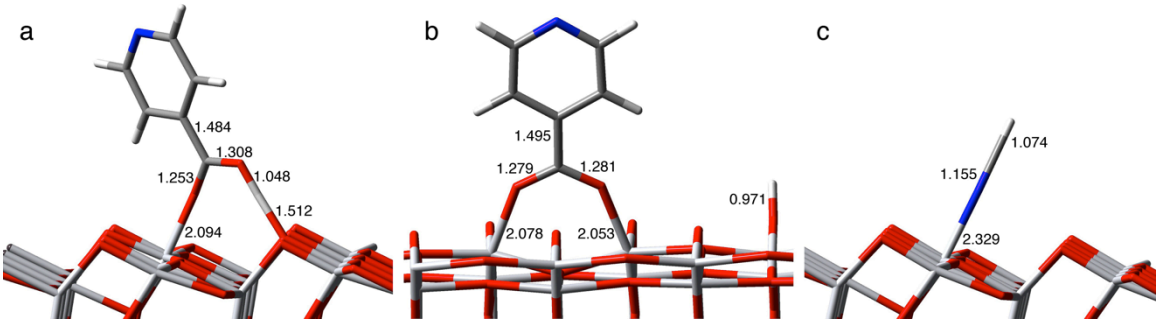

Figure 9. Optimized structures of anatase (101) with pyridine-4-carboxylic acid binding via a monodentate (a) and bidentate (b) binding mode, and hydrogen cyanide (c).

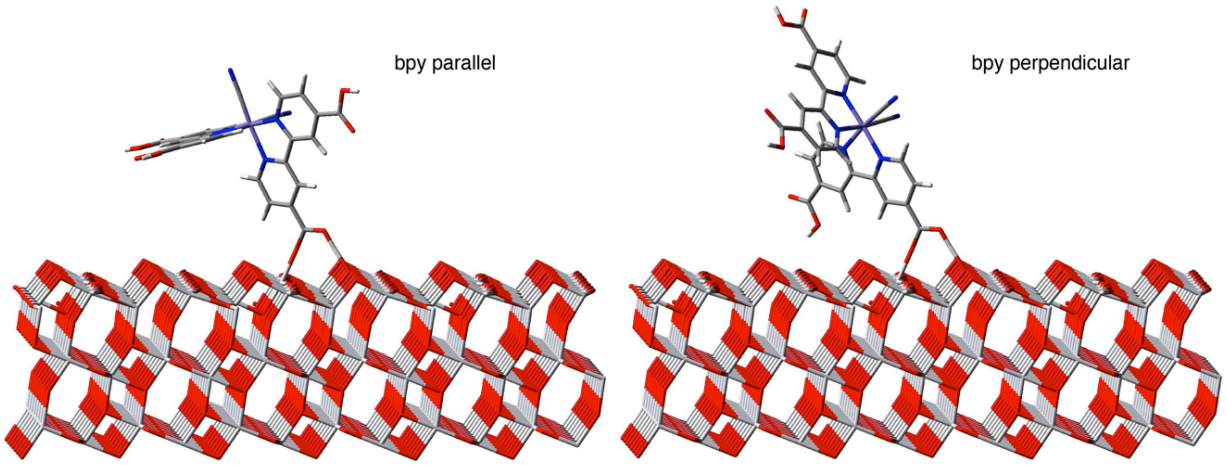

Figure 10. Final slab models of dye-nanoparticle assemblies consisting of $[Fe(bpy\text{-}dca)_2(CN)_2]$ attached to anatase (101) via a monodentate carboxylic acid binding mode in the following nonequivalent orientations: bpy parallel (left) and bpy perpendicular (right).

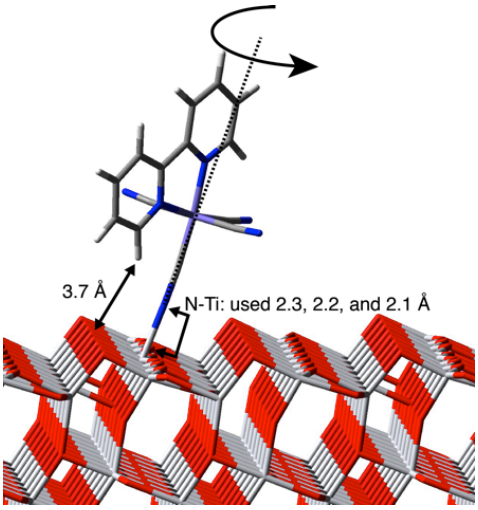

Figure 11. Structure of **1**-TiO_2 assembly employing CN^- as the anchoring group.

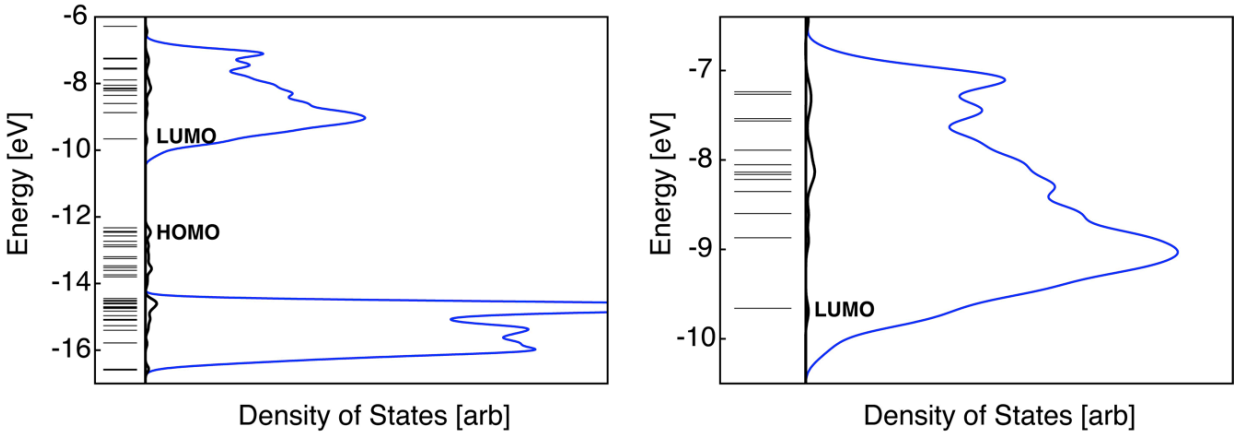

Figure 12. Density of states for **1**-TiO_2 anatase (101) slab model (left) and enlarged conduction band (right) show the following: total density of states (blue line), projected density of states on the dye (black line), and the energy levels of the dye in vacuum using extended Hückel (black level set lines). Gaussian line-shape (HWHM = 0.05 eV) used for convolution.

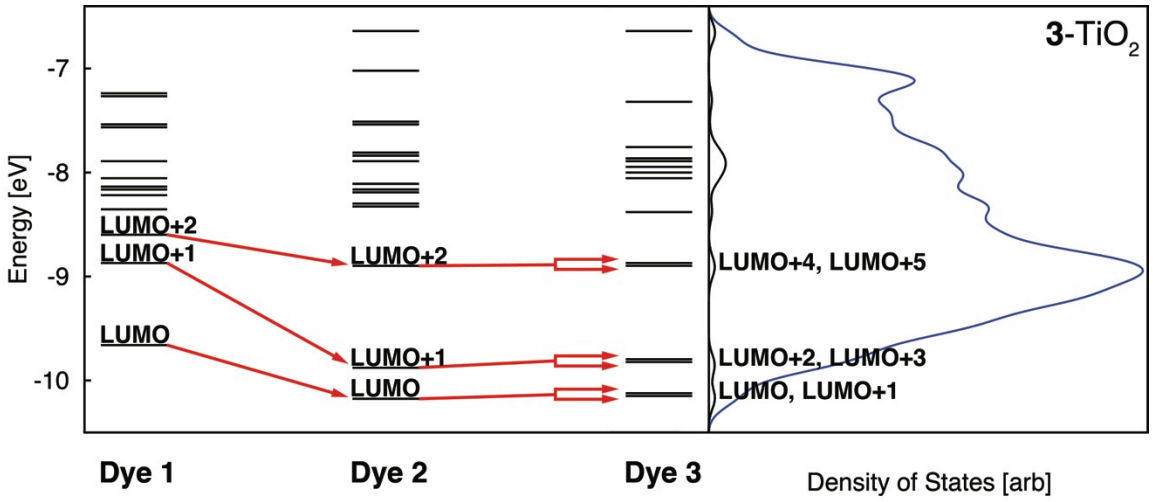

Figure 13. Discrete energy levels of the dyes (left) in vacuum, using extended Hückel level of theory, showing the evolution of the similar molecular orbitals, going from the smallest to the largest dye. The DOS/pDOS for the $[Fe(bpy\text{-}dca)_2(CN)_2]/TiO_2$ nanoparticle system is shown for reference (right).

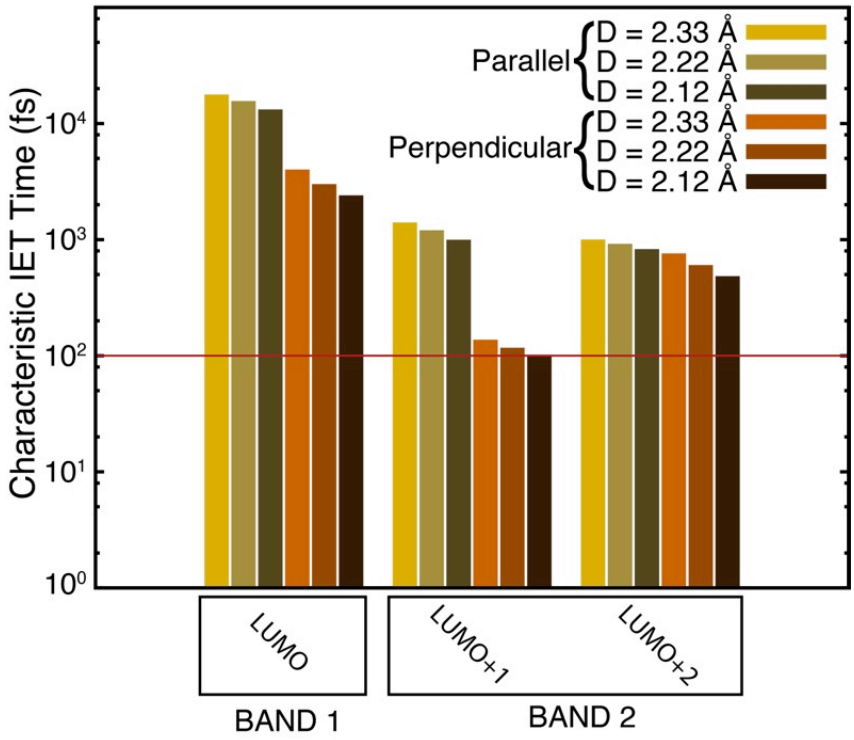

Figure 14. Characteristic interfacial electron transfer times for relevant particle states of $[Fe(bpy)(CN)_4]^{2-}$ attached to anatase (101) slab in both the "bpy parallel" and "bpy perpendicular" orientations via monodentate cyanide anchoring groups with varying nitrogen titanium distances (2.33, 2.22, and 2.12 Å), determined by either exponential or biexponential fitting.

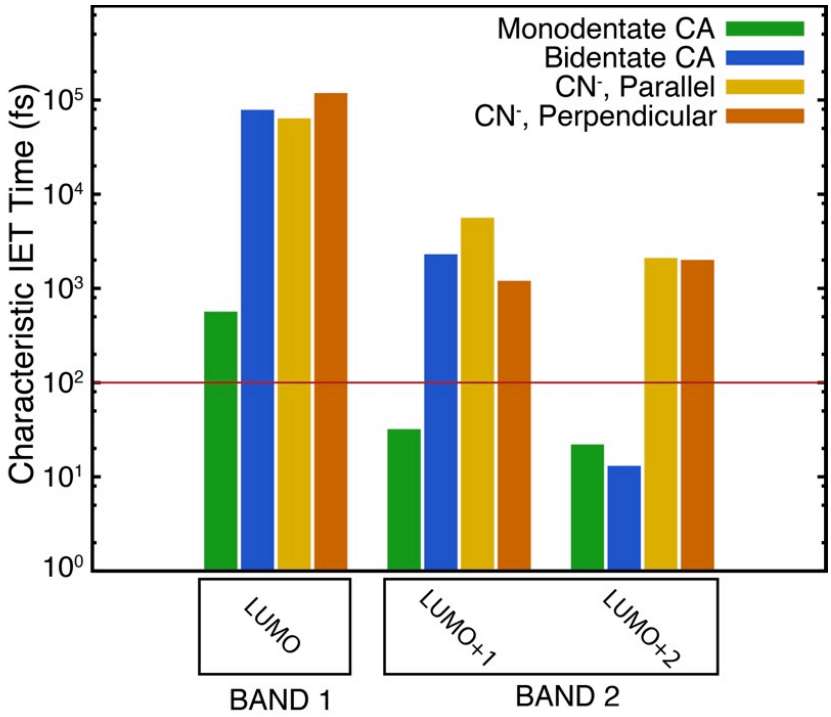

Figure 15. Characteristic interfacial electron transfer times for relevant particle states of [Fe(bpy-dca)$(CN)_4]^{2-}$ attached to anatase (101) slab by monodentate carboxylic acid, bidentate carboxylic acid, and cyanide anchoring groups (in both the "bpy parallel" and "bpy perpendicular" orientations), determined by either exponential or biexponential fitting.

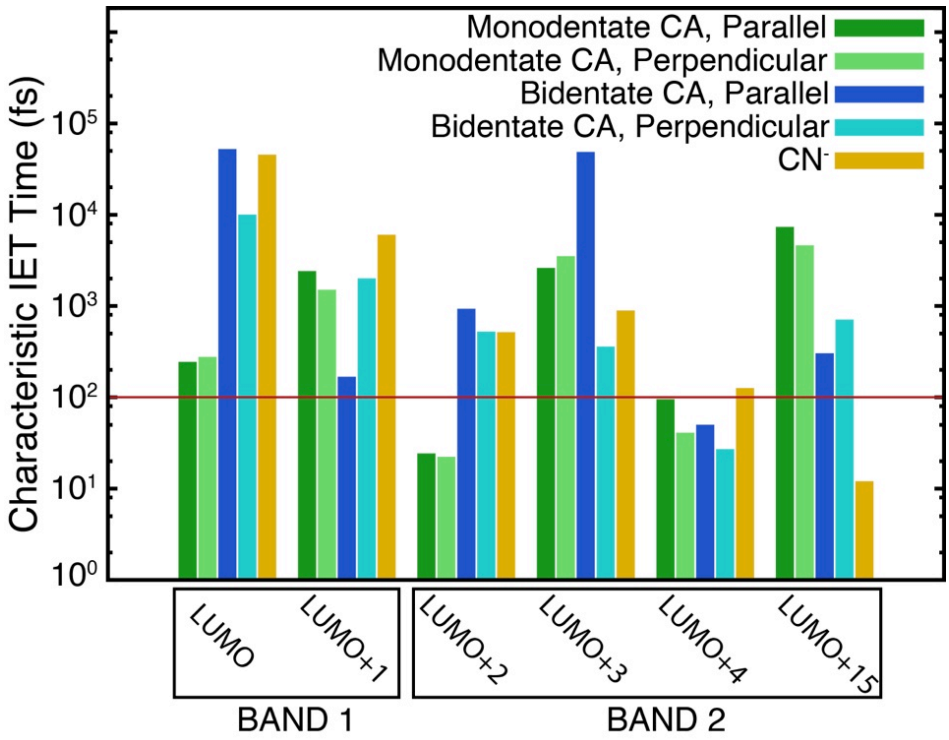

Figure 16. Characteristic interfacial electron transfer times for relevant particle states of $[Fe(bpy\text{-}dca)_2(CN)_2]$ attached to anatase (101) slab by monodentate carboxylic acid (in both the "bpy parallel" and "bpy perpendicular" orientations), bidentate carboxylic acid (in both the "bpy parallel" and "bpy perpendicular" orientations), and cyanide anchoring groups, determined by either exponential or biexponential fitting.